Guaranteed methods based on constrained zonotopes for set-valued state estimation of nonlinear discrete-time systems☆

Brenner S. Rego [a,*], Guilherme V. Raffo [a,b], Joseph K. Scott [c], Davide M. Raimondo [d]

[a] Graduate Program in Electrical Engineering, Federal University of Minas Gerais, Belo Horizonte, MG 31270-901, Brazil
[b] Department of Electronics Engineering, Federal University of Minas Gerais, Belo Horizonte, MG 31270-901, Brazil
[c] Department of Chemical and Biomolecular Engineering, Clemson University, Clemson, SC, USA
[d] Department of Electrical, Computer and Biomedical Engineering, University of Pavia, Italy

ARTICLE INFO

Keywords:
Nonlinear state estimation
Set-based computing
Reachability analysis
Convex polytopes

ABSTRACT

This paper presents new methods for set-valued state estimation of nonlinear discrete-time systems with unknown-but-bounded uncertainties. A single time step involves propagating an enclosure of the system states through the nonlinear dynamics (prediction), and then enclosing the intersection of this set with a bounded-error measurement (update). When these enclosures are represented by simple sets such as intervals, ellipsoids, parallelotopes, and zonotopes, certain set operations can be very conservative. Yet, using general convex polytopes is much more computationally demanding. To address this, we present in this paper two new methods, a mean value extension and a first-order Taylor extension, for efficiently propagating constrained zonotopes through nonlinear mappings. These extend existing methods for zonotopes in a consistent way. Examples show that these extensions yield tighter prediction enclosures than zonotopic estimation methods, while largely retaining the computational benefits of zonotopes. Moreover, they enable tighter update enclosures because constrained zonotopes can represent intersections much more accurately than zonotopes.

1. Introduction

The importance of state estimation has become evident in many fields of research over the years. Examples of recurrent applications are the localization problem (Jaulin, 2009a; Saeedi, Trentini, Seto, & Li, 2016), state-feedback control (Goodarzi & Lee, 2017; Jaulin, 2009b; Santos, Rego, Raffo, & Ferramosca, 2017), and fault detection and isolation (FDI) (Combastel, Zhang, & Lalami, 2008; Raimondo, Marseglia, Braatz, & Scott, 2016; Zhao, Huang, & Liu, 2015). If stochastic descriptions of the process and measurement uncertainties are available, then Bayesian state estimation methods such as Kalman filtering or particle filtering are typically employed. On the other hand, if only bounds on the uncertainties are known, then set-valued state estimation methods are applied (Chisci, Garulli, & Zappa, 1996; Jaulin, 2009b; Le, Stoica, Alamo, Camacho, & Dumur, 2013; Rego & Raffo, 2019; Rego, Raimondo, & Raffo, 2018a). Recent approaches also consider the presence of both kinds of uncertainties in the system (Combastel, 2015).

Set-valued state estimation methods aim to construct compact sets that are guaranteed to enclose all possible trajectories of the system subject to unknown-but-bounded uncertainties (Alamo, Bravo, & Camacho, 2005; Chisci et al., 1996). Using the standard recursive approach for discrete-time systems, this involves first bounding the image of the current enclosure under the dynamics (prediction), and then enclosing the intersection of this set with the set of states consistent with a bounded-error measurement (update). For discrete-time linear systems, if the initial set is a polytope, then exact enclosures can in principle be computed using convex polytopes (Girard & Guernic, 2008). However, even for linear dynamics, polytope propagation requires demanding operations (e.g., polytope projection, Minkowski sum, or conversion between vertex and halfspace representations) whose complexity grows dramatically with time due to the complexity increase of the resulting sets (Shamma & Tu, 1999; Walter & Piet-Lahanier, 1989). For these reasons, enclosures are often described by simpler sets including ellipsoids (Durieu, Walter, & Polyak, 2001; Polyak, Nazin, Durieu, & Walter, 2004; Schweppe, 1968), parallelotopes (Chisci et al., 1996; Vicino & Zappa, 1996), zonotopes (Combastel, 2003; Le et al., 2013), or combinations

* Corresponding author.
E-mail addresses: brennersr7@ufmg.br (B.S. Rego), raffo@ufmg.br (G.V. Raffo), jks9@clemson.edu (J.K. Scott), davide.raimondo@unipv.it (D.M. Raimondo).

of these (Chabane, Maniu, Alamo, Camacho, & Dumur, 2014). However, the mathematical limitations of these sets require certain operations to be conservative, sometimes quite significantly. Notably, this includes set intersection, which is critical for the update step in set-valued state estimation (Chisci et al., 1996; Durieu et al., 2001; Le et al., 2013). The article Althoff and Krogh (2011) proposes the use of zonotope bundles to describe intersections of zonotopes without explicit computation. However, the Minkowski sum and linear image (see Section 3) are outer-approximated. In the article Scott, Raimondo, Marseglia, and Braatz (2016), *constrained zonotopes* are introduced to overcome many of the limitations of zonotopes. These sets are closed under intersection, Minkowski sum, and linear image, and are capable of describing arbitrary convex polytopes if the complexity of the set description is not limited. Efficient algorithms for linear set-valued state estimation and also FDI using constrained zonotopes are described in Raimondo et al. (2016) and Scott et al. (2016).

In contrast to the linear case, effective set-valued state estimation for nonlinear systems is still an open challenge (Alamo et al., 2005; Combastel, 2005; Jaulin, 2009b; Wan, Sharma, & Sutton, 2018). Early approaches in this field used inclusion functions based on interval arithmetic (Moore, Kearfott, & Cloud, 2009) to propagate bounds through the nonlinear dynamics, and used interval-based set inversion techniques to enclose the set of states consistent with the current measurement (Jaulin, 2009a, 2009b; Kieffer, Jaulin, & Walter, 1998). Improved accuracy is achieved using refinements (i.e., unions of intervals) as well as more advanced interval methods such as contractor and separator algebras (Jaulin, 2009a, 2016). Unfortunately, even these methods often provide conservative bounds without extensive refinement, which is only tractable for systems with relatively few states (Jaulin, 2009b). An interesting new interval method based on discrete-time differential inequalities is proposed in Yang and Scott (2018), but it only applies to Euler discretized systems with limited step size.

A few alternatives for nonlinear set-valued state estimation can be found in the literature. Polytopes are used in Shamma and Tu (1997) for systems with nonlinear dynamics and linear measurements. The prediction step is performed based on a linearization of the dynamics, in which conservative interval enclosures are used to bound the linearization error. Notably, the computed error bound is valid for any value of the state, rather than being computed as a function of the current state enclosure, which can lead to a very conservative result. Another issue with this method is that the complexity of the polytopic enclosures grows rapidly with time, which results in a very high computational burden because the complexity of the required set operations scales poorly with increasing polytope complexity. More efficient methods based on zonotopes are proposed in Alamo et al. (2005) and Combastel (2005). The propagation step in Alamo et al. (2005) is based on the Mean Value Theorem and is referred to as the *mean value extension*, while the approach in Combastel (2005) uses a first-order Taylor expansion with a rigorous remainder bound, and is referred to as the *first-order Taylor extension*. Updates are then achieved by methods for outer-approximating the intersection of a zonotope with a strip (i.e., a linear measurement with bounded error). An alternative zonotope-based prediction step using DC programming is proposed in Alamo, Bravo, Redondo, and Camacho (2008), but with the same intersection method as in Bravo, Alamo, and Camacho (2006). Even for linear measurements, the symmetry of zonotopes is known to cause significant errors in the update step (Scott et al., 2016). General convex polytopes in halfspace representation are used in Wan et al. (2018) to enable an exact update. Prediction is then done by representing the polytope as an intersection of zonotopes and applying the mean value extension. Unfortunately, conversion between these representations is computationally demanding, and the increasing complexity of the zonotope bundle with time is not addressed. Constrained zonotopes have recently been applied to nonlinear state estimation in Rego, Raimondo, and Raffo (2018b) and shown to provide much higher accuracy than existing zonotopic methods. Nevertheless, the method in Rego et al. (2018b) uses an interval partitioning scheme and is therefore intractable for high-dimensional systems. Finally, in an effort to overcome the limitations of convex sets, polynomial zonotopes are introduced in Althoff (2013) and used for reachability analysis. However, update algorithms for polynomial zonotopes have not been developed.

In this context, the main contributions of this paper are two new methods for nonlinear set-valued state estimation based on constrained zonotopes. We follow the standard algorithmic steps typically used for set-valued state estimation (i.e., prediction, update, and reduction). For the prediction step, we use new generalizations of the mean value extension and first-order Taylor extension discussed above that enable constrained zonotopes, rather than zonotopes, to be effectively propagated through nonlinear discrete-time dynamics. Since this class of sets corresponds to an alternative representation of convex polytopes, these generalizations can be viewed as novel approaches for implicitly propagating convex polytopes through nonlinear mappings. The generalization of these methods to constrained zonotopes is not straightforward and requires significant modifications to the existing proofs. However, it results in much tighter prediction enclosures than existing zonotopic methods in some cases, as shown in the numerical examples. Moreover, using constrained zonotopes for prediction also enables the update step to be done much more effectively using the generalized intersection operation for constrained zonotopes. On the other hand, reduction becomes more complex than for zonotopes, leading to interesting trade-offs between accuracy and computational efficiency. We investigate these trade-offs both through numerical examples and by developing a detailed computational complexity analysis of the proposed methods and their zonotopic counterparts. To the best of our knowledge, such an analysis has not been conducted previously for either zonotopes or constrained zonotopes in the context of nonlinear set-valued estimation.

The remainder of the paper is organized as follows. The nonlinear set-valued state estimation problem is stated in Section 2. Essential mathematical background is presented in Section 3, including a discussion of constrained zonotopes and their main properties. Section 4 develops the main results of the paper; namely, the proposed mean value and first-order Taylor extensions for constrained zonotopes, heuristics for selecting the point at which the approximation is performed, and the computational complexity analysis. Numerical examples are presented in Section 5 to demonstrate the effectiveness of these extensions for set-valued state estimation of nonlinear discrete-time systems. Finally, Section 6 concludes the paper.

2. Problem formulation

Consider a class of discrete-time systems with nonlinear dynamics and linear measurements, described by

$$\begin{aligned} \mathbf{x}_k &= \mathbf{f}(\mathbf{x}_{k-1}, \mathbf{u}_{k-1}, \mathbf{w}_{k-1}), \\ \mathbf{y}_k &= \mathbf{C}\mathbf{x}_k + \mathbf{D}_u\mathbf{u}_k + \mathbf{D}_v\mathbf{v}_k, \end{aligned} \tag{1}$$

for $k \geq 1$, with $\mathbf{y}_0 = \mathbf{C}\mathbf{x}_0 + \mathbf{D}_u\mathbf{u}_0 + \mathbf{D}_v\mathbf{v}_0$, where $\mathbf{x}_k \in \mathbb{R}^n$ denotes the system state, $\mathbf{u}_k \in \mathbb{R}^{n_u}$ is a known input, $\mathbf{w}_k \in \mathbb{R}^{n_w}$ is the process disturbance, $\mathbf{y}_k \in \mathbb{R}^{n_y}$ is the measured output, and $\mathbf{v}_k \in \mathbb{R}^{n_v}$ is the measurement uncertainty, with $\mathbf{x}_0$ the initial state. The nonlinear mapping $\mathbf{f}$ is assumed to be of class $\mathcal{C}^2$, and the disturbances and uncertainties are assumed to be bounded, i.e., $\mathbf{w}_k \in W_k$ and $\mathbf{v}_k \in V_k$, where W_k and V_k are known compact sets.

This work proposes new methods to perform set-valued state estimation for nonlinear systems as in (1). The exact characterization of sets X_k containing the evolution of the system states is very difficult in the nonlinear case, if not intractable (Kieffer et al., 1998; Kühn, 1998; Platzer & Clarke, 2007). Therefore, in the set-membership framework the objective is to enclose such sets as tightly as possible by guaranteed outer bounds $\hat{X}_k$ on the possible trajectories of the system states $\mathbf{x}_k$. Such outer bounds must be consistent with the previous estimate $\hat{X}_{k-1}$, known inputs $\mathbf{u}_{k-1}$, the current measurement $\mathbf{y}_k$, and also with the bounds on the disturbances and uncertainties W_{k-1}, V_k. Given an initial condition $\mathbf{x}_0 \in \hat{X}_0$, a common approach is to proceed through the well-known prediction–update algorithm, which consists in computing compact sets $\bar{X}_k$ and $\hat{X}_k$ such that

$$\bar{X}_k \supseteq \{\mathbf{f}(\mathbf{x}, \mathbf{u}_{k-1}, \mathbf{w}) : \mathbf{x} \in \hat{X}_{k-1},\ \mathbf{w} \in W_{k-1}\}, \tag{2}$$

$$\hat{X}_k \supseteq \{\mathbf{x} \in \bar{X}_k : \mathbf{C}\mathbf{x} + \mathbf{D}_u\mathbf{u}_k + \mathbf{D}_v\mathbf{v} = \mathbf{y}_k,\ \mathbf{v} \in V_k\}, \tag{3}$$

in which (2) is referred to as the *prediction step*, and (3) as the *update step*.

Our goal is to obtain accurate outer bounds $\bar{X}_k$ and $\hat{X}_k$ according to (2) and (3), respectively. Following these definitions, and considering the initial condition $\mathbf{x}_0 \in \hat{X}_0$, the property $\mathbf{x}_k \in \hat{X}_k$ is guaranteed by construction for all $k \geq 1$ (Alamo et al., 2008; Chisci et al., 1996; Le et al., 2013).

3. Preliminaries

3.1. Set operations and constrained zonotopes

A few common set operations are often used to compute enclosures satisfying (2) and (3) (Le et al., 2013; Scott et al., 2016). Consider $Z, W \subset \mathbb{R}^n$, $\mathbf{R} \in \mathbb{R}^{m\times n}$, and $Y \subset \mathbb{R}^m$. Define the linear mapping, Minkowski sum, and generalized intersection, as

$$\mathbf{R}Z \triangleq \{\mathbf{R}\mathbf{z} : \mathbf{z} \in Z\}, \tag{4}$$

$$Z \oplus W \triangleq \{\mathbf{z} + \mathbf{w} : \mathbf{z} \in Z,\ \mathbf{w} \in W\}, \tag{5}$$

$$Z \cap_{\mathbf{R}} Y \triangleq \{\mathbf{z} \in Z : \mathbf{R}\mathbf{z} \in Y\}, \tag{6}$$

respectively. Using ellipsoids or parallelotopes, the linear mapping (4) can be computed exactly, but (5) and (6) must be over-approximated (Chisci et al., 1996; Schweppe, 1968). For intervals, the Minkowski sum (5) is exact, but (4) and (6) are conservative due to the wrapping effect.[1] In contrast, convex polytopes are closed under (4)–(6). Moreover, (4) and (5) can be computed efficiently in vertex representation (V-rep), and (6) can be computed efficiently in half-space representation (H-rep). However, conversion between H-rep and V-rep is computationally expensive. Zonotopes (Kühn, 1998) allow (4) and (5) to be computed exactly and with low computational burden, but (6) is not a zonotope in general and must be over-approximated (Bravo et al., 2006; Le et al., 2013).

Constrained zonotopes are an extension of zonotopes, recently proposed in Scott et al. (2016), and are the class of sets of main interest in this work.

Definition 1. A set $Z \subset \mathbb{R}^n$ is a *constrained zonotope* if there exists $(\mathbf{G}_z, \mathbf{c}_z, \mathbf{A}_z, \mathbf{b}_z) \in \mathbb{R}^{n\times n_g} \times \mathbb{R}^n \times \mathbb{R}^{n_c\times n_g} \times \mathbb{R}^{n_c}$ such that

$$Z = \{\mathbf{c}_z + \mathbf{G}_z\boldsymbol{\xi} : \|\boldsymbol{\xi}\|_\infty \leq 1, \mathbf{A}_z\boldsymbol{\xi} = \mathbf{b}_z\}. \tag{7}$$

Eq. (7) is called *constrained generator representation* (CG-rep), in which each column of $\mathbf{G}_z$ is a *generator*, $\mathbf{c}_z$ is the *center*, and $\mathbf{A}_z\boldsymbol{\xi} = \mathbf{b}_z$ are *constraints*. In this work, we refer to $\boldsymbol{\xi}$ as the *generator variables*. Let $B_\infty(\mathbf{A}_z, \mathbf{b}_z) = \{\boldsymbol{\xi} \in \mathbb{R}^{n_g} : \|\boldsymbol{\xi}\|_\infty \leq 1,\ \mathbf{A}_z\boldsymbol{\xi} = \mathbf{b}_z\}$ and $B_\infty^{n_g} = \{\boldsymbol{\xi} \in \mathbb{R}^{n_g} : \|\boldsymbol{\xi}\|_\infty \leq 1\}$ be, respectively, the constrained unitary hypercube and the n_g-dimensional unitary hypercube.[2] Then, a constrained zonotope Z can alternatively be interpreted as an affine transformation of $B_\infty(\mathbf{A}_z, \mathbf{b}_z)$, given by $Z = \mathbf{c}_z \oplus \mathbf{G}_z B_\infty(\mathbf{A}_z, \mathbf{b}_z)$. Note that the linear equality constraints in (7) allow constrained zonotopes to represent any convex polytope provided that the complexity of the CG-rep (7) is not limited. In fact, Z is a constrained zonotope iff it is a convex polytope (Scott et al., 2016). We use the compact notation $Z = \{\mathbf{G}_z, \mathbf{c}_z, \mathbf{A}_z, \mathbf{b}_z\}$ for constrained zonotopes, and $Z = \{\mathbf{G}_z, \mathbf{c}_z\}$ for zonotopes.

In addition to (4) and (5), the intersection (6) can also be computed exactly with constrained zonotopes. Let $Z = \{\mathbf{G}_z, \mathbf{c}_z, \mathbf{A}_z, \mathbf{b}_z\} \subset \mathbb{R}^n$, $W = \{\mathbf{G}_w, \mathbf{c}_w, \mathbf{A}_w, \mathbf{b}_w\} \subset \mathbb{R}^n$, $Y = \{\mathbf{G}_y, \mathbf{c}_y, \mathbf{A}_y, \mathbf{b}_y\} \subset \mathbb{R}^m$, and $\mathbf{R} \in \mathbb{R}^{m\times n}$. The set operations (4)–(6) are computed in CG-rep as

$$\mathbf{R}Z = \{\mathbf{R}\mathbf{G}_z, \mathbf{R}\mathbf{c}_z, \mathbf{A}_z, \mathbf{b}_z\}, \tag{8}$$

$$Z \oplus W = \left\{\begin{bmatrix}\mathbf{G}_z & \mathbf{G}_w\end{bmatrix}, \mathbf{c}_z + \mathbf{c}_w, \begin{bmatrix}\mathbf{A}_z & \mathbf{0}\\ \mathbf{0} & \mathbf{A}_w\end{bmatrix}, \begin{bmatrix}\mathbf{b}_z\\ \mathbf{b}_w\end{bmatrix}\right\}, \tag{9}$$

$$Z \cap_{\mathbf{R}} Y = \left\{\begin{bmatrix}\mathbf{G}_z & \mathbf{0}\end{bmatrix}, \mathbf{c}_z, \begin{bmatrix}\mathbf{A}_z & \mathbf{0}\\ \mathbf{0} & \mathbf{A}_y\\ \mathbf{R}\mathbf{G}_z & -\mathbf{G}_y\end{bmatrix}, \begin{bmatrix}\mathbf{b}_z\\ \mathbf{b}_y\\ \mathbf{c}_y - \mathbf{R}\mathbf{c}_z\end{bmatrix}\right\}. \tag{10}$$

These operations can be performed efficiently and cause only a moderate increase in the complexity of the CG-rep. Other useful operations with constrained zonotopes are presented in the following. Property 1 provides a simple method for computing the interval hull of a constrained zonotope by solving $2n$ linear programs (LPs), while Proposition 1 provides a way to obtain the closest point in a constrained zonotope to another point in space (in the 1-norm sense) through the solution of a single LP. For simplicity, the subscripts of the variables in (7) will be suppressed henceforth when not necessary.

Property 1 (*Rego et al., 2018b; Scott et al., 2016*)**.** *Let $Z = \{\mathbf{G}, \mathbf{c}, \mathbf{A}, \mathbf{b}\} \subset \mathbb{R}^n$ and let $\mathbf{G}_j$ denote the jth row of $\mathbf{G}$. The* interval hull *$[\boldsymbol{\zeta}^{\mathrm{L}}, \boldsymbol{\zeta}^{\mathrm{U}}] \supseteq Z$ is obtained by solving the following linear programs for each $j = 1, 2, \ldots, n$:*

$$\zeta_j^{\mathrm{L}} = \min_{\boldsymbol{\xi}} \left\{c_j + \mathbf{G}_j\boldsymbol{\xi} : \|\boldsymbol{\xi}\|_\infty \leq 1,\ \mathbf{A}\boldsymbol{\xi} = \mathbf{b}\right\},$$

$$\zeta_j^{\mathrm{U}} = \max_{\boldsymbol{\xi}} \left\{c_j + \mathbf{G}_j\boldsymbol{\xi} : \|\boldsymbol{\xi}\|_\infty \leq 1,\ \mathbf{A}\boldsymbol{\xi} = \mathbf{b}\right\}.$$

Proposition 1. *Let $Z = \{\mathbf{G}, \mathbf{c}, \mathbf{A}, \mathbf{b}\} \subset \mathbb{R}^n$ and $\mathbf{h} \in \mathbb{R}^n$. A point $\mathbf{z} \in Z$ that minimizes $\|\mathbf{z} - \mathbf{h}\|_1$ is given by $\mathbf{z}^* = \mathbf{c} + \mathbf{G}\boldsymbol{\xi}^*$, where $\boldsymbol{\xi}^*$ is a solution to the linear program*

$$\min_{\boldsymbol{\xi}} \|\mathbf{c} - \mathbf{h} + \mathbf{G}\boldsymbol{\xi}\|_1 \quad \text{s.t.} \quad \mathbf{A}\boldsymbol{\xi} = \mathbf{b}, \quad \|\boldsymbol{\xi}\|_\infty \leq 1.$$

Proof. By definition,

$$\|\mathbf{z}^* - \mathbf{h}\|_1 = \|\mathbf{c} - \mathbf{h} + \mathbf{G}\boldsymbol{\xi}^*\|_1 \leq \|\mathbf{c} - \mathbf{h} + \mathbf{G}\boldsymbol{\xi}\|_1, \quad \forall \boldsymbol{\xi} \in B_\infty(\mathbf{A}, \mathbf{b}).$$

But, for any $\mathbf{z} \in Z$, there exists $\boldsymbol{\xi} \in B_\infty(\mathbf{A}, \mathbf{b})$ such that $\mathbf{z} = \mathbf{c} + \mathbf{G}\boldsymbol{\xi}$. Therefore, $\|\mathbf{z}^* - \mathbf{h}\|_1 \leq \|\mathbf{z} - \mathbf{h}\|_1$, $\forall \mathbf{z} \in Z$. ■

The presence of the equality constraints in (7) may result in $\mathbf{c}_z \notin Z$ (from $Z = \mathbf{c}_z \oplus \mathbf{G}_z B_\infty(\mathbf{A}_z, \mathbf{b}_z)$, $\mathbf{c}_z \notin Z$ as long as $\nexists \boldsymbol{\xi} \in B_\infty(\mathbf{A}_z, \mathbf{b}_z)$ satisfying $\mathbf{G}_z\boldsymbol{\xi} = \mathbf{0}$). Some of the techniques proposed in this paper require that $\mathbf{c}_z \in Z$ (Section 4.3). To accommodate this, Proposition 2 provides a simple method for computing an alternative (more complex) CG-rep for Z whose center is any desired point in space.

[1] The generalized intersection in (6) is not conservative when $\mathbf{R} = \mathbf{I}$, which corresponds to the standard intersection $\cap$.

[2] For simplicity, we drop the use of the superscript n_g for $B_\infty(\mathbf{A}_z, \mathbf{b}_z)$. This dimension can be directly inferred from the number of columns of $\mathbf{A}_z$.

Proposition 2 (*Rescaling with Desired Center*). *Let* $Z = \{\mathbf{G}, \mathbf{c}, \mathbf{A}, \mathbf{b}\} \subset \mathbb{R}^n$ *and let* $\tilde{\boldsymbol{\xi}}^{\mathrm{L}}, \tilde{\boldsymbol{\xi}}^{\mathrm{U}} \in \mathbb{R}^{n_g}$ *satisfy* $B_\infty(\mathbf{A}, \mathbf{b}) \subseteq [\tilde{\boldsymbol{\xi}}^{\mathrm{L}}, \tilde{\boldsymbol{\xi}}^{\mathrm{U}}]$. *Choose any desired center* $\mathbf{h} \in \mathbb{R}^n$ *lying in the range of* $\mathbf{G}$ *and let* $\boldsymbol{\xi}^{\mathrm{L}}, \boldsymbol{\xi}^{\mathrm{U}} \in \mathbb{R}^{n_g}$ *be solutions to the linear program:*

$$\min_{\boldsymbol{\xi}^{\mathrm{L}}, \boldsymbol{\xi}^{\mathrm{U}}} \left\| \frac{1}{2}(\boldsymbol{\xi}^{\mathrm{U}} - \boldsymbol{\xi}^{\mathrm{L}}) \right\|_1$$
$$\text{s.t.} \quad \mathbf{c} + \frac{1}{2}\mathbf{G}(\boldsymbol{\xi}^{\mathrm{L}} + \boldsymbol{\xi}^{\mathrm{U}}) = \mathbf{h}, \quad \boldsymbol{\xi}^{\mathrm{L}} \leq \tilde{\boldsymbol{\xi}}^{\mathrm{L}}, \quad \boldsymbol{\xi}^{\mathrm{U}} \geq \tilde{\boldsymbol{\xi}}^{\mathrm{U}}.$$

Letting $\boldsymbol{\xi}_{\mathrm{m}} = \frac{1}{2}(\boldsymbol{\xi}^{\mathrm{L}} + \boldsymbol{\xi}^{\mathrm{U}})$ *and* $\mathbf{E}_r = \frac{1}{2}\mathrm{diag}(\boldsymbol{\xi}^{\mathrm{U}} - \boldsymbol{\xi}^{\mathrm{L}})$, *an equivalent CG-rep of* Z *with center* $\mathbf{h}$ *is given by*

$$Z = \left\{ \begin{bmatrix} \mathbf{G}\mathbf{E}_r & \mathbf{0} \end{bmatrix}, \mathbf{h}, \begin{bmatrix} \mathbf{A}\mathbf{E}_r & \mathbf{0} \\ \mathbf{0} & \mathbf{A} \\ \mathbf{G}\mathbf{E}_r & -\mathbf{G} \end{bmatrix}, \begin{bmatrix} \mathbf{b} - \mathbf{A}\boldsymbol{\xi}_{\mathrm{m}} \\ \mathbf{b} \\ \mathbf{c} - \mathbf{h} \end{bmatrix} \right\}. \tag{11}$$

Proof. It is first shown that Z is contained in the set

$$\bar{Z} = \{\mathbf{G}\mathbf{E}_r,\ \mathbf{c} + \mathbf{G}\boldsymbol{\xi}_{\mathrm{m}},\ \mathbf{A}\mathbf{E}_r,\ \mathbf{b} - \mathbf{A}\boldsymbol{\xi}_{\mathrm{m}}\}.$$

Choose any $\mathbf{z} \in Z$. There must exist $\boldsymbol{\xi} \in B_\infty(\mathbf{A}, \mathbf{b})$ such that $\mathbf{z} = \mathbf{c} + \mathbf{G}\boldsymbol{\xi}$. Since $\boldsymbol{\xi} \in [\boldsymbol{\xi}^{\mathrm{L}}, \boldsymbol{\xi}^{\mathrm{U}}]$, there must exist $\boldsymbol{\delta} \in B_\infty^{n_g}$ such that $\boldsymbol{\xi} = \boldsymbol{\xi}_{\mathrm{m}} + \mathbf{E}_r\boldsymbol{\delta}$. Thus,

$$\mathbf{z} \in Z \implies \exists \boldsymbol{\delta} \in B_\infty^{n_g} : \mathbf{z} = \mathbf{c} + \mathbf{G}(\boldsymbol{\xi}_{\mathrm{m}} + \mathbf{E}_r\boldsymbol{\delta}),$$
$$\mathbf{A}(\boldsymbol{\xi}_{\mathrm{m}} + \mathbf{E}_r\boldsymbol{\delta}) = \mathbf{b} \implies \mathbf{z} \in \bar{Z}.$$

Therefore, $Z \subseteq \bar{Z}$ and it is true that $Z = \bar{Z} \cap Z$. Since $\boldsymbol{\xi}^{\mathrm{L}}$ and $\boldsymbol{\xi}^{\mathrm{U}}$ satisfy $\mathbf{c} + \frac{1}{2}\mathbf{G}(\boldsymbol{\xi}^{\mathrm{L}} + \boldsymbol{\xi}^{\mathrm{U}}) = \mathbf{c} + \mathbf{G}\boldsymbol{\xi}_{\mathrm{m}} = \mathbf{h}$, then representing $\bar{Z} \cap Z$ as in (10) gives (11). ■

Remark 1. The linear program in Proposition 2 does not require $[\boldsymbol{\xi}^{\mathrm{L}}, \boldsymbol{\xi}^{\mathrm{U}}] \subseteq B_\infty^{n_g}$. Therefore, the midpoint $\frac{1}{2}(\boldsymbol{\xi}^{\mathrm{L}} + \boldsymbol{\xi}^{\mathrm{U}})$ can assume any desired value, and it is always possible to satisfy $\mathbf{c} + \frac{1}{2}\mathbf{G}(\boldsymbol{\xi}^{\mathrm{L}} + \boldsymbol{\xi}^{\mathrm{U}}) = \mathbf{h}$ if $\mathbf{h}$ is in the range of $\mathbf{G}$. Thus, the linear program is feasible for all $\mathbf{h} \in \mathbb{R}^n$ if $\mathbf{G}$ is full row rank.

Remark 2. The optimization problems in this section can be readily rewritten as standard form LPs by using additional decision variables and constraints (Boyd & Vandenberghe, 2004).

4. Nonlinear state estimation

This section presents two new methods for set-valued state estimation of the class of nonlinear discrete-time systems described by (1). Focusing on the prediction step (2), we address the problem of propagating a constrained zonotope $\hat{X}_{k-1}$ through a nonlinear mapping, with $\hat{X}_0$, W_k, and V_k being constrained zonotopes as well. This is done by extending, in a consistent way, two existing approaches for propagating zonotopes through nonlinear mappings; namely, the *mean value extension* in Alamo et al. (2005) and Kühn (1998) and the *first-order Taylor extension* in Combastel (2005). The methods described in these works rely, respectively, on the Mean Value Theorem and Taylor's Theorem for the calculation of rigorous outer bounds of the range of the nonlinear mapping in order to obtain zonotopes enclosing the system trajectories. Both methods are based on intersection with strips for performing the update step (3). The key advantage of our new extensions is that they allow the entire state estimation procedure to be done using constrained zonotopes in CG-rep. Therefore, the update (3) can be done by generalized intersection (with linear measurements), which is known to generate highly asymmetrical sets that cannot be accurately enclosed by ellipsoids, intervals, parallelotopes, or zonotopes. Using the methods developed below, such sets can be directly propagated to the next time step without prior simplification to a symmetric set. This overcomes a major source of conservatism in existing methods based on the aforementioned enclosures, while largely retaining the efficiency of computations with zonotopes. In addition, our methods expand the use of the important tools developed in Scott et al. (2016) to the class of nonlinear discrete-time systems described in Section 2. In the remainder of the paper, functions with set-valued arguments are consistently used to denote exact image of the set under the function; e.g., $\boldsymbol{\mu}(X, W) \triangleq \{\boldsymbol{\mu}(\mathbf{x}, \mathbf{w}) : \mathbf{x} \in X,\ \mathbf{w} \in W\}$.

The methods below make use of interval arithmetic in several places. Here we recall some of its main concepts. Let $\mathbb{IR}$ denote the set of compact intervals in $\mathbb{R}$. Then $x \in \mathbb{IR}$ is a real compact set defined by $x = \{a \in \mathbb{R} : x^{\mathrm{L}} \leq a \leq x^{\mathrm{U}}\}$, with shorthand notation $[x^{\mathrm{L}}, x^{\mathrm{U}}]$. The midpoint and radius are defined by $\mathrm{mid}(x) = \frac{1}{2}(x^{\mathrm{U}} + x^{\mathrm{L}})$ and $\mathrm{rad}(x) = \frac{1}{2}(x^{\mathrm{U}} - x^{\mathrm{L}})$. The diameter is $\mathrm{diam}(x) = 2\mathrm{rad}(x)$. Interval vectors and matrices are defined by $\{\mathbf{a} \in \mathbb{R}^n : a_i^{\mathrm{L}} \leq a_i \leq a_i^{\mathrm{U}}\}$ and $\{\mathbf{A} \in \mathbb{R}^{n \times m} : A_{ij}^{\mathrm{L}} \leq A_{ij} \leq A_{ij}^{\mathrm{U}}\}$, respectively, with midpoint and radius defined component-wise. $\square(\mathbf{f}(X))$ denotes an interval enclosure of the range of a vector valued function $\mathbf{f}$ over $X \subset \mathbb{R}^n$. The notation $\square(\mathbf{f}(X))$ is used even when X is not an interval. In this case, it is assumed that the interval hull of X is employed in the operation. Inclusion functions satisfy $\mathbf{f}(X) \subseteq \square(\mathbf{f}(X))$. See Moore et al. (2009) for definitions of basic interval arithmetic operations and examples.

In addition, the following notations are defined to be used in our proofs. Let $\boldsymbol{\kappa}$ be a function of class $\mathcal{C}^2$ and $\mathbf{z}$ denote its argument. Then, κ_q denotes the qth component of $\boldsymbol{\kappa}$, $\nabla\boldsymbol{\kappa}$ denotes the gradient of $\boldsymbol{\kappa}$, and $\mathbf{H}\kappa_q$ is an upper triangular matrix describing half of the Hessian of κ_q. Specifically, $H_{ii}\kappa_q = (1/2)\partial^2\kappa_q/\partial z_i^2$, $H_{ij}\kappa_q = \partial^2\kappa_q/\partial z_i \partial z_j$ for $i < j$, and $H_{ij}\kappa_q = 0$ for $i > j$.

4.1. Mean value extension

This section presents the first of two new methods for enclosing the range of a nonlinear function $\boldsymbol{\mu}$ over a set of inputs described by constrained zonotopes. This method is referred to as the *mean value extension* of $\boldsymbol{\mu}$ (because it relies on the Mean Value Theorem), and is a consistent generalization of the method for zonotopes in Alamo et al. (2005). Due to significant differences with respect to its zonotopic counterpart, a new theorem (Theorem 2) together with a detailed proof is provided for the new method.

The method in Alamo et al. (2005) relies on a *zonotope inclusion* operator that computes a zonotopic enclosure of the product of an interval matrix with a unitary box. We first generalize this operator to constrained zonotopes.

Theorem 1. *Let* $X = \mathbf{p} \oplus \mathbf{M}B_\infty(\mathbf{A}, \mathbf{b}) \subset \mathbb{R}^m$ *be a constrained zonotope with* n_g *generators and* n_c *constraints, let* $\mathbf{J} \in \mathbb{IR}^{n \times m}$ *be an interval matrix, and consider the set* $S = \mathbf{J}X \triangleq \{\hat{\mathbf{J}}\mathbf{x} : \hat{\mathbf{J}} \in \mathbf{J}, \mathbf{x} \in X\} \subset \mathbb{R}^n$. *Let* $\bar{X} = \bar{\mathbf{p}} \oplus \bar{\mathbf{M}}B_\infty^{\bar{n}_g}$ *be a zonotope satisfying* $X \subseteq \bar{X}$, *let* $\mathbf{m}$ *be an interval vector such that* $\mathbf{m} \supseteq (\mathbf{J} - \mathrm{mid}(\mathbf{J}))\bar{\mathbf{p}}$ *and* $\mathrm{mid}(\mathbf{m}) = \mathbf{0}$, *and let* $\mathbf{P} \in \mathbb{R}^{n \times n}$ *be a diagonal matrix defined by*

$$P_{ii} = \frac{1}{2}\mathrm{diam}(m_i) + \frac{1}{2}\sum_{j=1}^{\bar{n}_g}\sum_{k=1}^{m}\mathrm{diam}(J_{ik})|\bar{M}_{kj}|, \tag{12}$$

for all $i = 1, 2, \ldots, n$. *Then* S *is contained in the* CZ-inclusion

$$S \subseteq \triangleleft(\mathbf{J}, X) \triangleq \mathrm{mid}(\mathbf{J})X \oplus \mathbf{P}B_\infty^n. \tag{13}$$

Proof. Choose any $\mathbf{s} \in S$. It will be shown that $\mathbf{s} \in \triangleleft(\mathbf{J}, X)$. By the definition of S, there must exist $\mathbf{x} \in X$ and $\hat{\mathbf{J}} \in \mathbf{J}$ such that $\mathbf{s} = \hat{\mathbf{J}}\mathbf{x}$. Adding and subtracting $\mathrm{mid}(\mathbf{J})\mathbf{x}$,

$$\mathbf{s} = \mathrm{mid}(\mathbf{J})\mathbf{x} + (\hat{\mathbf{J}} - \mathrm{mid}(\mathbf{J}))\mathbf{x}.$$

Since $\mathbf{x} \in X \subseteq \bar{X}$, there exists $\boldsymbol{\gamma} \in B_\infty^{\bar{n}_g}$ such that $\mathbf{x} = \bar{\mathbf{p}} + \bar{\mathbf{M}}\boldsymbol{\gamma}$. Therefore, $\mathbf{s} = \text{mid}(\mathbf{J})\mathbf{x} + (\hat{\mathbf{J}} - \text{mid}(\mathbf{J}))(\bar{\mathbf{p}} + \bar{\mathbf{M}}\boldsymbol{\gamma})$. By the choice of $\mathbf{m}$, there must exist $\hat{\mathbf{m}} \in \mathbf{m}$ such that

$$\mathbf{s} = \text{mid}(\mathbf{J})\mathbf{x} + \hat{\mathbf{m}} + (\hat{\mathbf{J}} - \text{mid}(\mathbf{J}))\bar{\mathbf{M}}\boldsymbol{\gamma}. \tag{14}$$

Let $\boldsymbol{\eta} = \hat{\mathbf{m}} + (\hat{\mathbf{J}} - \text{mid}(\mathbf{J}))\bar{\mathbf{M}}\boldsymbol{\gamma}$. Then

$$\begin{aligned}\eta_i &= \hat{m}_i + \sum_{j=1}^{\bar{n}_g}((\hat{\mathbf{J}} - \text{mid}(\mathbf{J}))\bar{\mathbf{M}})_{ij}\gamma_j,\\ &= \hat{m}_i + \sum_{j=1}^{\bar{n}_g}\left(\sum_{k=1}^{m}(\hat{J}_{ik} - \text{mid}(J_{ik}))\bar{M}_{kj}\right)\gamma_j.\end{aligned}$$

By the triangle inequality and the fact that $|\gamma_j| \leq 1$,

$$\begin{aligned}|\eta_i| &\leq |\hat{m}_i| + \sum_{j=1}^{\bar{n}_g}\left(\sum_{k=1}^{m}|(\hat{J}_{ik} - \text{mid}(J_{ik}))||\bar{M}_{kj}|\right)|\gamma_j|,\\ &\leq \frac{1}{2}\text{diam}(m_i) + \frac{1}{2}\sum_{j=1}^{\bar{n}_g}\sum_{k=1}^{m}\text{diam}(J_{ik})|\bar{M}_{kj}|.\end{aligned}$$

Therefore, $\boldsymbol{\eta} \in \mathbf{P}B_\infty^n$. From (14), this implies that

$$\mathbf{s} = \text{mid}(\mathbf{J})\mathbf{x} + \boldsymbol{\eta} \in \text{mid}(\mathbf{J})X \oplus \mathbf{P}B_\infty^n = \triangleleft(\mathbf{J}, X).$$

Thus $S \subseteq \triangleleft(\mathbf{J}, X)$. ■

Remark 3. In Theorem 1, a zonotope satisfying $X \subseteq \bar{X}$ can be easily obtained by performing n_c iterated constraint eliminations on X using the method in Scott et al. (2016). Moreover, $\mathbf{m}$ can be obtained by simply evaluating $(\mathbf{J} - \text{mid}(\mathbf{J}))\bar{\mathbf{p}}$ with interval arithmetic. These methods are used in this work. Finally, the enclosure (13) has $n_g + n$ generators and n_c constraints.

The following theorem provides the mean value extension for constrained zonotopes.

Theorem 2. *Let $\boldsymbol{\mu} : \mathbb{R}^n \times \mathbb{R}^{n_w} \to \mathbb{R}^n$ be continuously differentiable and $\nabla_x\boldsymbol{\mu}$ denote the gradient of $\boldsymbol{\mu}$ with respect to its first argument. Let $X \subset \mathbb{R}^n$ and $W \subset \mathbb{R}^{n_w}$ be constrained zonotopes and choose any $\mathbf{h} \in X$. If Z is a constrained zonotope such that $\boldsymbol{\mu}(\mathbf{h}, W) \subseteq Z$ and $\mathbf{J} \in \mathbb{IR}^{n\times n}$ is an interval matrix satisfying $\nabla_x^T\boldsymbol{\mu}(X, W) \subseteq \mathbf{J}$, then $\boldsymbol{\mu}(X, W) \subseteq Z \oplus \triangleleft(\mathbf{J}, X - \mathbf{h})$.*

Proof. Choose any $(\mathbf{x}, \mathbf{w}) \in X\times W$. It will be shown that $\boldsymbol{\mu}(\mathbf{x}, \mathbf{w}) \in Z \oplus \triangleleft(\mathbf{J}, X - \mathbf{h})$. For any $i = 1, 2, \ldots, n$, the Mean Value Theorem ensures that $\exists\boldsymbol{\delta}^{[i]} \in X$ such that

$$\mu_i(\mathbf{x}, \mathbf{w}) = \mu_i(\mathbf{h}, \mathbf{w}) + \nabla_x^T\mu_i(\boldsymbol{\delta}^{[i]}, \mathbf{w})(\mathbf{x} - \mathbf{h}).$$

But the vector $\nabla_x^T\mu_i(\boldsymbol{\delta}^{[i]}, \mathbf{w})$ is contained in the ith row of $\mathbf{J}$ by hypothesis, and since this is true for all $i = 1, 2, \ldots, n$, there exists a real matrix $\hat{\mathbf{J}} \in \mathbf{J}$ such that $\boldsymbol{\mu}(\mathbf{x}, \mathbf{w}) = \boldsymbol{\mu}(\mathbf{h}, \mathbf{w}) + \hat{\mathbf{J}}(\mathbf{x} - \mathbf{h})$.

By Theorem 1 and the choice of Z, it follows that $\boldsymbol{\mu}(\mathbf{x}, \mathbf{w}) \in Z \oplus \triangleleft(\mathbf{J}, X - \mathbf{h})$, as desired. ■

Remark 4. The interval matrix $\mathbf{J}$ required by Theorem 2 can be obtained by computing the interval hulls of X and W as in Property 1 and then bounding $\nabla_x^T\boldsymbol{\mu}(X, W)$ using interval arithmetic. Similarly, the constrained zonotope $Z \supseteq \boldsymbol{\mu}(\mathbf{h}, W)$ can be obtained by bounding $\boldsymbol{\mu}(\mathbf{h}, W)$ with interval arithmetic. Alternatively, another mean value extension can be applied around some $\mathbf{h}_w \in W$ to obtain $\boldsymbol{\mu}(\mathbf{h}, W) \subseteq Z \triangleq \boldsymbol{\mu}(\mathbf{h}, \mathbf{h}_w) \oplus \triangleleft(\mathbf{J}_w, W - \mathbf{h}_w)$, where $\mathbf{J}_w$ is an interval enclosure of $\nabla_w^T\boldsymbol{\mu}(\mathbf{h}, W)$. Finally, if $\boldsymbol{\mu}$ is affine in $\mathbf{w}$, i.e., $\boldsymbol{\mu}(\mathbf{x}, \mathbf{w}) \triangleq \boldsymbol{\beta}_x(\mathbf{x}) + \mathbf{B}_w(\mathbf{x})\mathbf{w}$, then an exact enclosure of $\boldsymbol{\mu}(\mathbf{h}, W)$ is $Z = \boldsymbol{\beta}_x(\mathbf{h}) \oplus \mathbf{B}_w(\mathbf{h})W$.

Since the CG-rep (7) is an alternative representation for convex polytopes (Scott et al., 2016), the mean value extension developed in Theorem 2 provides a new method for propagating convex polytopes implicitly through nonlinear mappings. A related approach can be found in Wan et al. (2018), where convex polytopes are represented by intersections of zonotopes (i.e., zonotope bundles (Althoff & Krogh, 2011)). However, while effective complexity reduction algorithms are available for constrained zonotopes (Scott et al., 2016), efficient methods for complexity control of zonotope bundles have not yet been proposed.

Remark 5. The enclosure obtained in Theorem 2 has at most $n_g + n_{g_w} + 2n$ generators and $n_c + n_{c_w}$ constraints (considering Z computed as in the alternatives presented in Remark 4), with n_g and n_{g_w} denoting the number of generators of X and W, and n_c and n_{c_w} the number of constraints, respectively. Thus, the complexity of the resulting set grows linearly with respect to the number of constraints and generators.

4.2. First-order Taylor extension

This section presents the second new method for enclosing the range of a nonlinear function $\boldsymbol{\eta}$ over a set of inputs described by constrained zonotopes. This method is referred to as the *first-order Taylor extension* of $\boldsymbol{\eta}$ (because it relies on a first-order Taylor expansion with a rigorous remainder bound), and is a consistent generalization of the method for zonotopes in Combastel (2005). In contrast to Theorem 2, for the sake of simplicity of the proof, this function has only one argument. Even so, it is possible to consider both states and process uncertainties by concatenating them into a single vector. Due to substantial changes with respect to the zonotopic method, the new approach comes with a new theorem (Theorem 3) and a detailed proof. In the main result below, $(\cdot)_{i,:}$ denotes the ith row of a matrix, and $(\cdot)_{ij}$ denotes the element from its ith row and jth column.

Theorem 3. *Let $\boldsymbol{\eta} : \mathbb{R}^m \to \mathbb{R}^n$ be of class $\mathcal{C}^2$ and $\mathbf{z} \in \mathbb{R}^m$ denote its argument. Let $Z = \{\mathbf{G}, \mathbf{c}, \mathbf{A}, \mathbf{b}\} \subset \mathbb{R}^m$ be a constrained zonotope with m_g generators and m_c constraints. For each $q = 1, 2, \ldots, n$, let $\mathbf{Q}^{[q]} \in \mathbb{IR}^{m\times m}$ and $\tilde{\mathbf{Q}}^{[q]} \in \mathbb{IR}^{m_g\times m_g}$ be interval matrices satisfying $\mathbf{Q}^{[q]} \supseteq \mathbf{H}\eta_q(Z)$ and $\tilde{\mathbf{Q}}^{[q]} \supseteq \mathbf{G}^T\mathbf{Q}^{[q]}\mathbf{G}$. Moreover, define*

$$\tilde{c}_q = \text{trace}\left\{\text{mid}(\tilde{\mathbf{Q}}^{[q]})\right\}/2,$$

$$\tilde{\mathbf{G}}_{q,:} = \Big[\cdots \underbrace{\text{mid}(\tilde{Q}_{ii}^{[q]})/2}_{\forall i} \cdots \underbrace{\left(\text{mid}(\tilde{Q}_{ij}^{[q]}) + \text{mid}(\tilde{Q}_{ji}^{[q]})\right)}_{\forall i<j} \cdots\Big],$$

$$\tilde{\mathbf{G}}_{\mathbf{d}} = \text{diag}(\mathbf{d}), \quad d_q = \sum_{i,j}\left|\text{rad}(\tilde{Q}_{ij}^{[q]})\right|,$$

$$\tilde{\mathbf{A}} = \left[\tilde{\mathbf{A}}_\zeta \;\; \tilde{\mathbf{A}}_{\tilde{\boldsymbol{\xi}}} \;\; \mathbf{0}_{\frac{m_c}{2}(1+m_c)\times n}\right],$$

$$\tilde{\mathbf{A}}_\zeta = \underbrace{\begin{bmatrix}\vdots\\ \cdots \;\; \frac{1}{2}A_{ri}A_{si} \;\; \cdots\\ \vdots\end{bmatrix}}_{\forall i}\Big\downarrow \forall r\leq s,$$

$$\tilde{\mathbf{A}}_{\tilde{\boldsymbol{\xi}}} = \underbrace{\begin{bmatrix}\vdots\\ \cdots \;\; A_{ri}A_{sj} + A_{rj}A_{si} \;\; \cdots\\ \vdots\end{bmatrix}}_{\forall i<j}\Big\downarrow \forall r\leq s,$$

$$\tilde{\mathbf{b}} = \begin{bmatrix} \vdots \\ b_r b_s - \frac{1}{2}\sum_i A_{ri}A_{si} \\ \vdots \end{bmatrix} \Big\downarrow \forall r \le s,$$

with indices $i, j = 1, 2, \dots, m_g$ *and* $r, s = 1, 2, \dots, m_c$. *Finally, choose any* $\mathbf{h} \in Z$ *and let* $\mathbf{L} \in \mathbb{IR}^{n\times m}$ *be an interval matrix satisfying* $\mathbf{L}_{q,:} \supseteq (\mathbf{c}-\mathbf{h})^T\mathbf{Q}^{[q]}$ *for all* $q = 1, \dots, n$. *Then,*

$$\boldsymbol{\eta}(Z) \subseteq \boldsymbol{\eta}(\mathbf{h}) \oplus \nabla^T\boldsymbol{\eta}(\mathbf{h})(Z-\mathbf{h}) \oplus R, \tag{15}$$

where $R = \tilde{\mathbf{c}} \oplus \begin{bmatrix}\tilde{\mathbf{G}} & \tilde{\mathbf{G}}_\mathbf{d}\end{bmatrix} B_\infty(\tilde{\mathbf{A}}, \tilde{\mathbf{b}}) \oplus \triangleleft(\mathbf{L}, (\mathbf{c}-\mathbf{h}) \oplus 2\mathbf{G}B_\infty(\mathbf{A}, \mathbf{b}))$.

Proof. Choose any $\mathbf{z} \in Z$ and $q \in \{1, \dots, n\}$. By Taylor's theorem applied to η_q with reference point $\mathbf{h}$, there must exist $\boldsymbol{\Gamma}^{[q]} \in \mathbf{H}\eta_q(Z) \subseteq \mathbf{Q}^{[q]}$ such that[3]

$$\eta_q(\mathbf{z}) = \eta_q(\mathbf{h}) + \nabla^T\eta_q(\mathbf{h})(\mathbf{z}-\mathbf{h}) + (\mathbf{z}-\mathbf{h})^T\boldsymbol{\Gamma}^{[q]}(\mathbf{z}-\mathbf{h}).$$

Since $\mathbf{z} \in Z$, there must exist $\boldsymbol{\xi} \in B_\infty(\mathbf{A}, \mathbf{b})$ such that $\mathbf{z} = \mathbf{c} + \mathbf{G}\boldsymbol{\xi}$. Thus, defining $\mathbf{p} = \mathbf{c} - \mathbf{h}$ for brevity,

$$\eta_q(\mathbf{z}) = \eta_q(\mathbf{h}) + \nabla^T\eta_q(\mathbf{h})(\mathbf{p}+\mathbf{G}\boldsymbol{\xi}) + (\mathbf{p}+\mathbf{G}\boldsymbol{\xi})^T\boldsymbol{\Gamma}^{[q]}(\mathbf{p}+\mathbf{G}\boldsymbol{\xi}).$$

Expanding the product $(\mathbf{p}+\mathbf{G}\boldsymbol{\xi})^T\boldsymbol{\Gamma}^{[q]}(\mathbf{p}+\mathbf{G}\boldsymbol{\xi})$ yields $\mathbf{p}^T\boldsymbol{\Gamma}^{[q]}(\mathbf{p}+2\mathbf{G}\boldsymbol{\xi}) + \boldsymbol{\xi}^T\tilde{\boldsymbol{\Gamma}}^{[q]}\boldsymbol{\xi}$, with $\tilde{\boldsymbol{\Gamma}}^{[q]} = \mathbf{G}^T\boldsymbol{\Gamma}^{[q]}\mathbf{G} \in \tilde{\mathbf{Q}}^{[q]}$. Since $\tilde{\boldsymbol{\Gamma}}^{[q]} \in \tilde{\mathbf{Q}}^{[q]}$, it follows that $\tilde{\Gamma}_{ij}^{[q]} = \mathrm{mid}(\tilde{Q}_{ij}^{[q]}) + \mathrm{rad}(\tilde{Q}_{ij}^{[q]})\Lambda_{ij}^{[q]}$ for some $\Lambda_{ij}^{[q]} \in B_\infty^1$. Additionally, $\xi_i \in [-1, 1]$ implies that $\xi_i^2 \in [0, 1]$, and hence $\xi_i^2 = \frac{1}{2} + \frac{1}{2}\zeta_i$ for some $\zeta_i \in [-1, 1]$. Considering these two facts,

$$\begin{aligned}\boldsymbol{\xi}^T\tilde{\boldsymbol{\Gamma}}^{[q]}\boldsymbol{\xi} = &\frac{1}{2}\sum_i \mathrm{mid}(\tilde{Q}_{ii}^{[q]}) + \frac{1}{2}\sum_i \mathrm{mid}(\tilde{Q}_{ii}^{[q]})\zeta_i \\ &+ \sum_{i<j}(\mathrm{mid}(\tilde{Q}_{ij}^{[q]}) + \mathrm{mid}(\tilde{Q}_{ji}^{[q]}))\xi_i\xi_j + \sum_{i,j}\mathrm{rad}(\tilde{Q}_{ij}^{[q]})\xi_i\xi_j\Lambda_{ij}^{[q]},\end{aligned}$$

where the third summation results from the fact that $\xi_i\xi_j = \xi_j\xi_i$. Thus, by defining the new generator variables

$$\bar{\boldsymbol{\xi}} = \Big[\ \cdots\ \underbrace{\zeta_i}_{\forall i}\ \cdots\ \underbrace{\xi_i\xi_j}_{\forall i<j}\ \cdots\ \underbrace{\xi_i\xi_j\Lambda_{ij}^{[q]}}_{\forall i,j,q}\ \cdots\ \Big]^T,$$

with $i, j = 1, 2, \dots, m_g$, $q = 1, 2, \dots, n$, we have that $\boldsymbol{\xi}^T\tilde{\boldsymbol{\Gamma}}^{[q]}\boldsymbol{\xi} = \tilde{c}_q + [\tilde{\mathbf{G}}\ \ \bar{\mathbf{G}}_\mathbf{d}]_{q,:}\bar{\boldsymbol{\xi}}$, where $\bar{\mathbf{G}}_\mathbf{d} = \mathrm{blkdiag}(\mathbf{N}^{[1]}, \mathbf{N}^{[2]}, \dots, \mathbf{N}^{[n]})$,[4]

$$\mathbf{N}^{[q]} = \Big[\ \cdots\ \underbrace{\mathrm{rad}(\tilde{Q}_{ij}^{[q]})}_{\forall i,j}\ \cdots\ \Big] \in \mathbb{R}^{1\times m_g^2}.$$

Therefore, we have established that $\eta_q(\mathbf{z}) = \eta_q(\mathbf{h}) + \nabla^T\eta_q(\mathbf{h})(\mathbf{z}-\mathbf{h}) + \mathbf{p}^T\boldsymbol{\Gamma}^{[q]}(\mathbf{p}+2\mathbf{G}\boldsymbol{\xi}) + \tilde{c}_q + [\tilde{\mathbf{G}}\ \ \bar{\mathbf{G}}_\mathbf{d}]_{q,:}\bar{\boldsymbol{\xi}}$. This holds for every $q = 1, 2, \dots, n$. Moreover, $\mathbf{L}$ satisfies $\mathbf{L}_{q,:} \supseteq \mathbf{p}^T\mathbf{Q}^{[q]}$ for all $q = 1, 2, \dots, n$ by definition, so there must exist $\hat{\mathbf{L}} \in \mathbf{L}$ such that $\hat{\mathbf{L}}_{q,:} = \mathbf{p}^T\boldsymbol{\Gamma}^{[q]}$ for all $q = 1, 2, \dots, n$. Therefore,

$$\boldsymbol{\eta}(\mathbf{z}) = \boldsymbol{\eta}(\mathbf{h}) + \nabla^T\boldsymbol{\eta}(\mathbf{h})(\mathbf{z}-\mathbf{h}) + \hat{\mathbf{L}}(\mathbf{p}+2\mathbf{G}\boldsymbol{\xi}) + \tilde{\mathbf{c}} + [\tilde{\mathbf{G}}\ \ \bar{\mathbf{G}}_\mathbf{d}]\bar{\boldsymbol{\xi}}. \tag{16}$$

Furthermore, the equality constraints $\mathbf{A}\boldsymbol{\xi} = \mathbf{b}$ imply that $\mathbf{A}\boldsymbol{\xi}\boldsymbol{\xi}^T\mathbf{A}^T = \mathbf{b}\mathbf{b}^T$. Thus, considering $\xi_i^2 = \frac{1}{2} + \frac{1}{2}\zeta_i$, the rth row and sth column of this matrix equality yields

$$\frac{1}{2}\sum_i A_{ri}A_{si}\zeta_i + \sum_{i<j}(A_{ri}A_{sj} + A_{rj}A_{si})\xi_i\xi_j = b_r b_s - \frac{1}{2}\sum_i A_{ri}A_{si},$$

with $r, s = 1, 2, \dots, m_c$. Such constraints are linear in $\bar{\boldsymbol{\xi}}$, and non-repeating for $r \le s$, therefore $\bar{\mathbf{A}}\bar{\boldsymbol{\xi}} = \tilde{\mathbf{b}}$ holds, where $\bar{\mathbf{A}} = [\tilde{\mathbf{A}}_\zeta\ \ \tilde{\mathbf{A}}_\xi\ \ \mathbf{0}_{\tilde{m}_c\times nm_g^2}]$, with $\tilde{m}_c = \frac{m_c}{2}(1+m_c)$. Hence $\boldsymbol{\xi} \in B_\infty(\mathbf{A}, \mathbf{b}) \implies \bar{\boldsymbol{\xi}} \in B_\infty(\bar{\mathbf{A}}, \tilde{\mathbf{b}})$. Combining this with (16), we have proven the enclosure $\boldsymbol{\eta}(Z) \subseteq \boldsymbol{\eta}(\mathbf{h}) \oplus \nabla^T\boldsymbol{\eta}(\mathbf{h})(Z-\mathbf{h}) \oplus \mathbf{L}(\mathbf{p} \oplus 2\mathbf{G}B_\infty(\mathbf{A}, \mathbf{b})) \oplus \tilde{\mathbf{c}} \oplus [\tilde{\mathbf{G}}\ \ \bar{\mathbf{G}}_\mathbf{d}]B_\infty(\bar{\mathbf{A}}, \tilde{\mathbf{b}})$.

In fact, this enclosure can be greatly simplified by noting that the columns of $\bar{\mathbf{A}}$ corresponding to the variables $[\ \cdots\ \xi_i\xi_j\Lambda_{ij}^{[q]}\ \cdots\ ]$ are all zero, and hence

$$[\tilde{\mathbf{G}}\ \ \bar{\mathbf{G}}_\mathbf{d}]B_\infty(\bar{\mathbf{A}}, \tilde{\mathbf{b}}) = \tilde{\mathbf{G}}B_\infty([\tilde{\mathbf{A}}_\zeta\ \ \tilde{\mathbf{A}}_\xi], \tilde{\mathbf{b}}) \oplus \bar{\mathbf{G}}_\mathbf{d}B_\infty^{nm_g^2}.$$

Since $\bar{\mathbf{G}}_\mathbf{d}$ is block diagonal and each $\mathbf{N}^{[q]}$ is a row vector, $\bar{\mathbf{G}}_\mathbf{d}B_\infty^{nm_g^2}$ is an interval, and is equivalent to $\tilde{\mathbf{G}}_\mathbf{d}B_\infty^n$, with $\tilde{\mathbf{G}}_\mathbf{d}$ defined as in the statement of the theorem. Thus,

$$\begin{aligned}[\tilde{\mathbf{G}}\ \ \bar{\mathbf{G}}_\mathbf{d}]B_\infty(\bar{\mathbf{A}}, \tilde{\mathbf{b}}) &= \tilde{\mathbf{G}}B_\infty([\tilde{\mathbf{A}}_\zeta\ \ \tilde{\mathbf{A}}_\xi], \tilde{\mathbf{b}}) \oplus \tilde{\mathbf{G}}_\mathbf{d}B_\infty^n, \\ &= [\tilde{\mathbf{G}}\ \ \tilde{\mathbf{G}}_\mathbf{d}]B_\infty([\tilde{\mathbf{A}}_\zeta\ \ \tilde{\mathbf{A}}_\xi\ \ \mathbf{0}_{\tilde{m}_c\times n}], \tilde{\mathbf{b}}) = [\tilde{\mathbf{G}}\ \ \tilde{\mathbf{G}}_\mathbf{d}]B_\infty(\tilde{\mathbf{A}}, \tilde{\mathbf{b}}).\end{aligned}$$

Therefore, $\boldsymbol{\eta}(Z) \subseteq \boldsymbol{\eta}(\mathbf{h}) \oplus \nabla^T\boldsymbol{\eta}(\mathbf{h})(Z-\mathbf{h}) \oplus \mathbf{L}(\mathbf{p} \oplus 2\mathbf{G}B_\infty(\mathbf{A}, \mathbf{b})) \oplus \tilde{\mathbf{c}} \oplus [\tilde{\mathbf{G}}\ \ \tilde{\mathbf{G}}_\mathbf{d}]B_\infty(\tilde{\mathbf{A}}, \tilde{\mathbf{b}})$, and (15) follows immediately from the definition of R. ■

Remark 6. Regarding the definitions of $\tilde{\mathbf{G}}$, $\tilde{\mathbf{A}}_\zeta$, $\tilde{\mathbf{A}}_\xi$, and $\tilde{\mathbf{b}}$ in Theorem 3, the ordering of the indices $i < j$ and $r \le s$ is irrelevant, as long as it is the same for all variables.

Remark 7. The interval matrices $\mathbf{Q}^{[q]}$ required by Theorem 3 can be obtained by computing the interval hull of Z (Property 1) and then bounding $\mathbf{H}\eta_q(Z)$ using interval arithmetic. Moreover, $\tilde{\mathbf{Q}}^{[q]}$ and $\mathbf{L}$ can be obtained by evaluating $\mathbf{G}^T\mathbf{Q}^{[q]}\mathbf{G}$ and $(\mathbf{c}-\mathbf{h})^T\mathbf{Q}^{[q]}$ using interval arithmetic.

As stated before, process disturbances can be taken into account in (15) by considering the augmented vector $\mathbf{z} = (\mathbf{x}, \mathbf{w})$ with $Z = X \times W \subset \mathbb{R}^{n+n_w}$ and $\mathbf{h} = (\mathbf{h}_x, \mathbf{h}_w) \in Z$. With $X = \{\mathbf{G}_x, \mathbf{c}_x, \mathbf{A}_x, \mathbf{b}_x\}$ and $W = \{\mathbf{G}_w, \mathbf{c}_w, \mathbf{A}_w, \mathbf{b}_w\}$, the Cartesian product Z is easily computed by

$$X \times W = \left\{\begin{bmatrix}\mathbf{G}_x & \mathbf{0} \\ \mathbf{0} & \mathbf{G}_w\end{bmatrix}, \begin{bmatrix}\mathbf{c}_x \\ \mathbf{c}_w\end{bmatrix}, \begin{bmatrix}\mathbf{A}_x & \mathbf{0} \\ \mathbf{0} & \mathbf{A}_w\end{bmatrix}, \begin{bmatrix}\mathbf{b}_x \\ \mathbf{b}_w\end{bmatrix}\right\}.$$

Remark 8. In Theorem 3, $\tilde{\mathbf{G}}$ has $\sum_{j=1}^{m_g} j = \frac{1}{2}m_g(m_g+1)$ columns, $\tilde{\mathbf{G}}_\mathbf{d} \in \mathbb{R}^{n\times n}$, $\tilde{\mathbf{A}}$ has $\sum_{s=1}^{m_c} s = \frac{1}{2}m_c(m_c+1)$ rows, and $\triangleleft(\mathbf{L}, (\mathbf{c}-\mathbf{h}) \oplus 2\mathbf{G}B_\infty(\mathbf{A}, \mathbf{b}))$ has m_g+n generators and m_c constraints (Remark 3). Therefore, the resulting enclosure in (15) has $\frac{1}{2}m_g^2 + \frac{5}{2}m_g + 2n$ generators and $\frac{1}{2}m_c^2 + \frac{5}{2}m_c$ constraints. If $Z = X \times W$, then the enclosure has $\frac{1}{2}(n_g+n_{g_w})^2 + \frac{5}{2}(n_g+n_{g_w}) + 2n$ generators and $\frac{1}{2}(n_c+n_{c_w})^2 + \frac{5}{2}(n_c+n_{c_w})$ constraints, which is a polynomial increase in complexity in terms of both generators and constraints.

4.3. Selection of h

The methods proposed in the previous sections require a choice of $\mathbf{h} \in X = \{\mathbf{G}_x, \mathbf{c}_x, \mathbf{A}_x, \mathbf{b}_x\}$ in order to compute a constrained zonotope enclosure for the prediction step (2). As shown in Section 5.1, this choice may drastically affect the accuracy of the obtained enclosure. In the mean value extension for intervals and zonotopes, a usual choice of $\mathbf{h} \in X$ is the center of X (Alamo et al., 2005; Moore et al., 2009). However, with constrained zonotopes, since the center of the CG-rep may not belong to X (see Section 3), a different point $\mathbf{h} \in X$ must be chosen. A simple and inexpensive choice is the center of the interval hull of X. Unfortunately, even this point may not belong to X in some cases.[5] Nevertheless, this choice can be applied rigorously by

[3] Let $\boldsymbol{\Upsilon}^{[q]}$ belong to the standard Hessian matrix of $\eta_q(Z)$. Then, $(1/2)(\mathbf{z}-\mathbf{h})^T\boldsymbol{\Upsilon}^{[q]}(\mathbf{z}-\mathbf{h}) = (\mathbf{z}-\mathbf{h})^T\boldsymbol{\Gamma}^{[q]}(\mathbf{z}-\mathbf{h})$ holds. See Combastel (2005) for a motivation on this approach.

[4] In this work $\mathrm{blkdiag}(\mathbf{A}, \mathbf{B}, \dots)$ denotes a block diagonal matrix with blocks $\mathbf{A}, \mathbf{B}, \dots$.

[5] An example is the polytope with vertices (0, 0, 0), (1, 1, 0), (0, 1, 0), (0, 1, 1).

simply checking $\mathbf{h} \in X$ beforehand by solving an LP (Scott et al., 2016).

In the following, we analyze alternative choices of $\mathbf{h} \in X$. Firstly, we focus on suitable choices valid for the mean value extension (Theorem 2). This extension relies on the CZ-inclusion (Theorem 1), and therefore requires the computation of a zonotope enclosing $X - \mathbf{h}$. In this work, we assume that this zonotope is computed through constraint eliminations (see Remark 3). Let $\{\mathbf{G}^{(\ell)}, \mathbf{c}^{(\ell)}, \mathbf{A}^{(\ell)}, \mathbf{b}^{(\ell)}\}$ denote the constrained zonotope obtained by reducing to ℓ the number of remaining constraints in $X - \mathbf{h}$. Following the constraint elimination algorithm in Scott et al. (2016), for each $\ell = n_c, n_c - 1, \dots, 1$, the remaining constraints $\mathbf{A}^{(\ell)}\boldsymbol{\xi} = \mathbf{b}^{(\ell)}$ are first preconditioned through Gauss–Jordan elimination with full pivoting and then subjected to a rescaling procedure before the next constraint is eliminated. The entire procedure can be represented by the following recursive equations (see Proposition 5 and the Appendix in Scott et al. (2016) for details), where $\bar{(\cdot)}$ denotes variables after preconditioning, $\tilde{(\cdot)}$ denotes variables after rescaling, and $\boldsymbol{\Lambda}_\mathrm{G}$, $\boldsymbol{\Lambda}_\mathrm{A}$, $\boldsymbol{\xi}_\mathrm{m}$, and $\boldsymbol{\xi}_\mathrm{r}$ are defined as in Scott et al. (2016):

$$\begin{aligned}
\tilde{\mathbf{c}}^{(\ell)} &= \mathbf{c}^{(\ell)} + \bar{\mathbf{G}}^{(\ell)}\boldsymbol{\xi}_\mathrm{m}^{(\ell)}, & \mathbf{c}^{(\ell-1)} &= \tilde{\mathbf{c}}^{(\ell)} + \boldsymbol{\Lambda}_\mathrm{G}^{(\ell)}\tilde{\mathbf{b}}^{(\ell)},\\
\tilde{\mathbf{G}}^{(\ell)} &= \bar{\mathbf{G}}^{(\ell)}\mathrm{diag}(\boldsymbol{\xi}_\mathrm{r}^{(\ell)}), & \mathbf{G}^{(\ell-1)} &= \tilde{\mathbf{G}}^{(\ell)} - \boldsymbol{\Lambda}_\mathrm{G}^{(\ell)}\tilde{\mathbf{A}}^{(\ell)},\\
\tilde{\mathbf{A}}^{(\ell)} &= \bar{\mathbf{A}}^{(\ell)}\mathrm{diag}(\boldsymbol{\xi}_\mathrm{r}^{(\ell)}), & \mathbf{A}^{(\ell-1)} &= \tilde{\mathbf{A}}^{(\ell)} - \boldsymbol{\Lambda}_\mathrm{A}^{(\ell)}\tilde{\mathbf{A}}^{(\ell)},\\
\tilde{\mathbf{b}}^{(\ell)} &= \bar{\mathbf{b}}^{(\ell)} - \bar{\mathbf{A}}^{(\ell)}\boldsymbol{\xi}_\mathrm{m}^{(\ell)}, & \mathbf{b}^{(\ell-1)} &= \tilde{\mathbf{b}}^{(\ell)} - \boldsymbol{\Lambda}_\mathrm{A}^{(\ell)}\tilde{\mathbf{b}}^{(\ell)}.
\end{aligned} \tag{17}$$

Careful examination of the algorithm in Scott et al. (2016) reveals that the actions taken during preconditioning, rescaling, and constraint elimination are all independent of the center of the original constrained zonotope, which in this case is $\mathbf{c}^{(n_c)} = \mathbf{c}_x - \mathbf{h}$. Therefore, with exception of the center, the variables $(\cdot)^{(\ell)}$ can be obtained by eliminating the constraints of X prior to choosing $\mathbf{h}$. Considering procedure (17), the following corollary provides a choice of $\mathbf{h}$ that leads to a tight enclosure by reducing the conservativeness of the CZ-inclusion $\triangleleft(\mathbf{J}, X - \mathbf{h})$.

Corollary 1. *Let $X = \{\mathbf{G}_x, \mathbf{c}_x, \mathbf{A}_x, \mathbf{b}_x\} \subset \mathbb{R}^n$, and consider $\boldsymbol{\mu}$, W, and $\mathbf{J}$ as defined in Theorem 2. Assume that $\bar{\mathbf{G}}^{(\ell)}$, $\boldsymbol{\xi}_m^{(\ell)}$, $\boldsymbol{\Lambda}_\mathrm{G}^{(\ell)}$, and $\tilde{\mathbf{b}}^{(\ell)}$ are obtained by eliminating all n_c constraints from X according to (17) and set*

$$\mathbf{h} = \mathbf{c}_x + \sum_{\ell=1}^{n_c}\left(\bar{\mathbf{G}}^{(\ell)}\boldsymbol{\xi}_\mathrm{m}^{(\ell)} + \boldsymbol{\Lambda}_\mathrm{G}^{(\ell)}\tilde{\mathbf{b}}^{(\ell)}\right). \tag{18}$$

Let $\bar{X} = \{\mathbf{G}^{(0)}, \mathbf{c}^{(0)}\}$ be obtained by eliminating all n_c constraints from $X - \mathbf{h}$ according to (17), let $\mathbf{m} \supseteq (\mathbf{J} - \mathrm{mid}(\mathbf{J}))\mathbf{c}^{(0)}$ be computed by standard interval arithmetic, and suppose that $\triangleleft(\mathbf{J}, X - \mathbf{h})$ is computed as in Theorem 1 with this choice of $\bar{X}$ and $\mathbf{m}$. Finally, let $Z \supseteq \boldsymbol{\mu}(\mathbf{h}, W)$. If $\mathbf{h} \in X$, then $\boldsymbol{\mu}(X, W) \subseteq Z \oplus \triangleleft(\mathbf{J}, X - \mathbf{h})$. Moreover, $\triangleleft(\mathbf{J}, X - \mathbf{h}) \subseteq \triangleleft(\mathbf{J}, X - \tilde{\mathbf{h}})$ for any $\tilde{\mathbf{h}} \in X$, $\tilde{\mathbf{h}} \neq \mathbf{h}$.

Proof. For $\mathbf{h} \in X$, $\boldsymbol{\mu}(X, W) \subseteq Z \oplus \triangleleft(\mathbf{J}, X - \mathbf{h})$ follows directly from Theorem 2. Now, let us show that $\triangleleft(\mathbf{J}, X - \mathbf{h}) \subseteq \triangleleft(\mathbf{J}, X - \tilde{\mathbf{h}})$ holds for any $\tilde{\mathbf{h}} \in X$, $\tilde{\mathbf{h}} \neq \mathbf{h}$. Recursive computation of (17) leads to

$$\mathbf{c}^{(0)} = \mathbf{c}^{(n_c)} + \sum_{\ell=1}^{n_c}\left(\bar{\mathbf{G}}^{(\ell)}\boldsymbol{\xi}_\mathrm{m}^{(\ell)} + \boldsymbol{\Lambda}_\mathrm{G}^{(\ell)}\tilde{\mathbf{b}}^{(\ell)}\right), \tag{19}$$

where $\mathbf{c}^{(n_c)} = \mathbf{c}_x - \mathbf{h}$. Therefore, $\mathbf{c}^{(0)} = \mathbf{0}$ iff $\mathbf{h}$ is given by (18), thus $\mathbf{m} = \mathbf{0}$, and $\mathrm{diam}(\mathbf{m}) = \mathbf{0}$. Note that in (12), $\bar{\mathbf{M}} \triangleq \mathbf{G}^{(0)}$ is invariant with respect to $\mathbf{h}$, and since $\mathbf{J} \supseteq \nabla_x^T \boldsymbol{\mu}(X, W)$, then $\mathbf{J}$ is also invariant with respect to $\mathbf{h}$. Consequently, the second term in (12) is not a function of $\mathbf{h}$. Therefore, $\mathbf{P}B_\infty^n \subseteq \tilde{\mathbf{P}}B_\infty^n = (1/2)\mathrm{diag}(\mathrm{diam}(\tilde{\mathbf{m}}))B_\infty^n \oplus \mathbf{P}B_\infty^n$, with $\tilde{\mathbf{m}}$ computed using $\tilde{\mathbf{h}} \in X$. The result then follows from (13). ■

By Corollary 1, the enclosure obtained in Theorem 2 is tightened by choosing $\mathbf{h}$ such that $\mathbf{c}^{(0)}$ is equal to zero. Unfortunately, the $\mathbf{h}$ given by (18) may not belong to X, so an alternative to obtain tight bounds is to reduce the size of the box $\mathbf{m}$ by solving

$$\min_{\mathbf{h}} \{\|\mathrm{diam}(\mathbf{m})\|_1 : \mathbf{h} \in X\}, \tag{20}$$

with $\mathbf{m} \supseteq (\mathbf{J} - \mathrm{mid}(\mathbf{J}))\bar{\mathbf{p}}$ computed using interval arithmetic, where $\bar{\mathbf{p}} \triangleq \mathbf{c}^{(0)}$. Recall that $\mathbf{c}^{(0)}$ is the center of the zonotope obtained by eliminating all the constraints of $X - \mathbf{h}$.

Lemma 1. *Let $X = \{\mathbf{G}_x, \mathbf{c}_x, \mathbf{A}_x, \mathbf{b}_x\} \subset \mathbb{R}^n$, $\mathbf{J} \in \mathbb{IR}^{n\times n}$. Assume that $\bar{\mathbf{G}}^{(\ell)}$, $\boldsymbol{\xi}_\mathrm{m}^{(\ell)}$, $\boldsymbol{\Lambda}_\mathrm{G}^{(\ell)}$, and $\tilde{\mathbf{b}}^{(\ell)}$ are obtained by eliminating all n_c constraints of X according to (17). Then $\mathbf{h} = \mathbf{c}_x + \mathbf{G}_x\boldsymbol{\xi}^*$ is the solution to (20) iff $\boldsymbol{\xi}^*$ is the solution to the linear program*

$$\min_{\boldsymbol{\xi}} \|\boldsymbol{\Theta}\bar{\mathbf{p}}\|_1, \quad \text{s.t.} \quad \mathbf{A}_x\boldsymbol{\xi} = \mathbf{b}_x, \quad \|\boldsymbol{\xi}\|_\infty \leq 1, \tag{21}$$

with $\bar{\mathbf{p}} = -\mathbf{G}_x\boldsymbol{\xi} + \sum_{\ell=1}^{n_c}\left(\bar{\mathbf{G}}^{(\ell)}\boldsymbol{\xi}_\mathrm{m}^{(\ell)} + \boldsymbol{\Lambda}_\mathrm{G}^{(\ell)}\tilde{\mathbf{b}}^{(\ell)}\right)$, $\Theta_{jj} = \sum_{i=1}^n \mathrm{diam}(J_{ij})$, and $\Theta_{ij} = 0$ for $i \neq j$.

Proof. Each element of $(\mathbf{J} - \mathrm{mid}(\mathbf{J})) \in \mathbb{IR}^{n\times n}$ is a symmetric interval satisfying $(J_{ij} - \mathrm{mid}(J_{ij})) = (1/2)\mathrm{diam}(J_{ij})[-1, 1]$, and for every $a \in \mathbb{R}$, $a[-1, 1] = |a|[-1, 1]$ holds. Therefore $m_i = \sum_{j=1}^n (1/2)\mathrm{diam}(J_{ij})|\bar{p}_j|[-1, 1]$. Consequently, $\mathrm{diam}(m_i) = \sum_{j=1}^n \mathrm{diam}(J_{ij})|\bar{p}_j|$, and

$$\begin{aligned}
\|\mathrm{diam}(\mathbf{m})\|_1 &= \sum_{i=1}^n\sum_{j=1}^n \mathrm{diam}(J_{ij})|\bar{p}_j| = \sum_{j=1}^n\left(\sum_{i=1}^n \mathrm{diam}(J_{ij})\right)|\bar{p}_j|\\
&= \sum_{j=1}^n \Theta_{jj}|\bar{p}_j| = \|\boldsymbol{\Theta}\bar{\mathbf{p}}\|_1.
\end{aligned}$$

The equality $\bar{\mathbf{p}} = -\mathbf{G}_x\boldsymbol{\xi} + \sum_{\ell=1}^{n_c}\left(\bar{\mathbf{G}}^{(\ell)}\boldsymbol{\xi}_\mathrm{m}^{(\ell)} + \boldsymbol{\Lambda}_\mathrm{G}^{(\ell)}\tilde{\mathbf{b}}^{(\ell)}\right)$ and the constraints in (21) follow directly from (19) and $\mathbf{h} \in X$. ■

Lemma 1 yields an optimal choice of $\mathbf{h} \in X$ that can be used in Theorem 2 to reduce conservatism in the CZ-inclusion, and requires only the solution of an LP. Note that formulating (21) requires the knowledge of $\bar{\mathbf{G}}^{(\ell)}$, $\boldsymbol{\xi}_\mathrm{m}^{(\ell)}$, $\boldsymbol{\Lambda}_\mathrm{G}^{(\ell)}$, and $\tilde{\mathbf{b}}^{(\ell)}$, which are obtained from the iterated constraint elimination process. As stated before, constraint elimination can be performed over X to obtain the required data prior to the solution of (21). Once the optimal $\mathbf{h}$ is obtained, constraint elimination can be repeated, or equivalently, the zonotope obtained using $\mathbf{h} = \mathbf{0}$ can simply be translated by $-\mathbf{h}$.

Remark 9. Note that if the $\mathbf{h}$ given by Corollary 1 belongs to X, then this coincides with the solution provided by Lemma 1.

We summarize the proposed choices of $\mathbf{h} \in X$ for use in Theorem 2 as follows:

- ***(C1)*** $\mathbf{h}$ is given by the center of the interval hull of X, if it satisfies $\mathbf{h} \in X$;
- ***(C2)*** $\mathbf{h}$ is obtained by solving (21).

We now focus on suitable choices valid for the first-order Taylor extension. As with the mean value extension, the usual choice of $\mathbf{h} \in X$ in first-order Taylor extensions for intervals and zonotopes is the center of X (Combastel, 2005; Moore et al., 2009). The next corollary shows that this choice leads to a tight enclosure if it belongs to X.

Corollary 2. *Let $Z = \{\mathbf{G}, \mathbf{c}, \mathbf{A}, \mathbf{b}\} = X \times W \subset \mathbb{R}^m$, and consider $\boldsymbol{\eta}$, $\tilde{\mathbf{c}}$, $\tilde{\mathbf{G}}$, $\tilde{\mathbf{G}}_\mathbf{d}$, $\tilde{\mathbf{A}}$, $\tilde{\mathbf{b}}$, $\mathbf{L}$, and $\mathbf{Q}^{[q]}$ as defined in Theorem 3, with $q \in \{1, 2, \dots, n\}$. If $\mathbf{h} = \mathbf{c} \in Z$, then $\boldsymbol{\eta}(Z) \subseteq \boldsymbol{\eta}(\mathbf{h}) \oplus \nabla^T\boldsymbol{\eta}(\mathbf{h})(Z - \mathbf{h}) \oplus \tilde{\mathbf{c}} \oplus \begin{bmatrix}\tilde{\mathbf{G}} & \tilde{\mathbf{G}}_\mathbf{d}\end{bmatrix} B_\infty(\tilde{\mathbf{A}}, \tilde{\mathbf{b}})$.*

Proof. For $\mathbf{h} = \mathbf{c}$, $\mathbf{L}_{q,:} \supseteq (\mathbf{c} - \mathbf{h})^T \mathbf{Q}^{[q]} = \mathbf{0}$, $q = 1, 2, \ldots, n$. Therefore $\mathbf{L} = \mathbf{0}$ holds, and $\triangleleft(\mathbf{L}, (\mathbf{c} - \mathbf{h}) \oplus 2\mathbf{G}B_\infty(\mathbf{A}, \mathbf{b})) = \mathbf{0}$. The result then follows from (15). ■

By inspecting Corollary 2, it is clear that the enclosure in (15) is tightened since $\triangleleft(\mathbf{L}, (\mathbf{c} - \mathbf{h}) \oplus 2\mathbf{G}B_\infty(\mathbf{A}, \mathbf{b})) = \mathbf{0}$. However, since this point may not belong to X, a good alternative may be to consider the closest point in X to its center, obtained by means of Proposition 1. By the definition of $\mathbf{L}$, this heuristic leads to smaller values of diam($\mathbf{L}$), and therefore reduces the size of $\triangleleft(\mathbf{L}, (\mathbf{c} - \mathbf{h}) \oplus 2\mathbf{G}B_\infty(\mathbf{A}, \mathbf{b}))$ (see (12)). A third option is to apply Proposition 2 to obtain an alternative CG-rep of X with any desired center. In this case, the new center is chosen as some point in X, $\bar{\mathbf{h}} \in X$, and then $\mathbf{h}$ is chosen as $\mathbf{h} = \bar{\mathbf{h}}$. A simple choice of new center $\bar{\mathbf{h}} \in X$ for such a procedure is the center of the interval hull of X. The proposed alternatives for use in Theorem 3 are summarized as follows:

(C3) $\mathbf{h}$ is given by the closest point in X to the center of X, computed through Proposition 1;

(C4) $\mathbf{h}$ is the center of X, if it satisfies $\mathbf{h} \in X$. Otherwise, $\bar{\mathbf{h}} \in X$ is chosen as the center of the interval hull of X, the center of X is moved to $\bar{\mathbf{h}}$ using Proposition 2, and $\mathbf{h}$ is given by $\mathbf{h} = \bar{\mathbf{h}}$.[6]

4.4. Update step

An enclosure for the prediction step (2) can be obtained in CG-rep using either Theorem 2 or Theorem 3. Therefore, due to linearity of the measurement in (1), an exact bound for the update step (3) can be directly obtained by computing the generalized intersection of two constrained zonotopes as follows. Given the prediction set $\bar{X}_k$, a constrained zonotope V describing bounds on measurement errors, the current input $\mathbf{u}_k$ and measurement $\mathbf{y}_k$, an exact enclosure for the update step is obtained using the definition (6), given by

$$\hat{X}_k = \bar{X}_k \cap_{\mathbf{c}} ((\mathbf{y}_k - \mathbf{D}_u \mathbf{u}_k) \oplus (-\mathbf{D}_v V)). \tag{22}$$

It is well known that the intersection in (22) cannot be computed exactly using zonotopes, and must be over-approximated (Alamo et al., 2005; Le et al., 2013). As a consequence, the enclosures of the system states obtained after many iterations of prediction and update may be quite conservative using zonotopes. However, with constrained zonotopes all operations in (22) are easily computed through (8)–(10). These will lead to an enclosure with $n_g + n_{g_v}$ generators, and $n_c + n_{c_v} + n_y$ constraints, where n_g and n_c are the number of generators and constraints of $\bar{X}_k$, respectively.

Remark 10. Iterated computations of the proposed extensions (Theorems 2 and 3) and (22) result in at most a quadratic increase in the complexity of the CG-rep (7). As with zonotopes, this can be effectively addressed using *order reduction* algorithms (Kopetzki, Schürmann, & Althoff, 2017; Yang & Scott, 2018) that over-approximate a constrained zonotope by another with lower complexity. Efficient methods for reducing the number of generators and constraints of the CG-rep (7) with reasonable conservativeness were proposed in Scott et al. (2016).

4.5. Complexity analysis

Table 1 shows the computational complexity[7] of our methods for the prediction and update steps, as well as complexity reduction to the same number of generators and constraints of the set prior to prediction. Specifically, we use the mean value extension (Theorem 2) and the first-order Taylor extension (Theorem 3) for the prediction steps, while the update steps are both given by the generalized intersection (22). These methods are denoted by CZMV and CZFO, respectively. The computational complexities of their zonotope counterparts are also presented for comparison, denoted analogously by ZMV and ZFO, which use the mean value approach in Alamo et al. (2005) and the first-order Taylor approach in Combastel (2005), respectively, for the prediction step. The update algorithm proposed in Bravo et al. (2006) is used for both ZMV and ZFO because it provided the best trade-off between accuracy and efficiency in our numerical experiments with zonotopes. Complexity reduction is applied after the update step in all four methods using the reduction methods in Scott et al. (2016) for constrained zonotopes and Method 4 in Yang and Scott (2018) for zonotopes. For constrained zonotopes, constraint elimination is performed prior to generator reduction. The complexities in Table 1 take into account the growth of the number of generators and constraints after each step (see Remarks 5 and 8). The dimensions in Table 1 are specified by the definitions $\hat{X}_{k-1} = \{\mathbf{G}_x, \mathbf{c}_x\}$, $W = \{\mathbf{G}_w, \mathbf{c}_w\}$, and $V = \{\mathbf{G}_v, \mathbf{c}_v\}$ or $\hat{X}_{k-1} = \{\mathbf{G}_x, \mathbf{c}_x, \mathbf{A}_x, \mathbf{b}_x\}$, $W = \{\mathbf{G}_w, \mathbf{c}_w, \mathbf{A}_w, \mathbf{b}_w\}$, and $V = \{\mathbf{G}_v, \mathbf{c}_v, \mathbf{A}_v, \mathbf{b}_v\}$ with $\mathbf{G}_x \in \mathbb{R}^{n \times n_g}$, $\mathbf{c}_x \in \mathbb{R}^n$, $\mathbf{A}_x \in \mathbb{R}^{n_c \times n_g}$, $\mathbf{b}_x \in \mathbb{R}^{n_c}$, $\mathbf{G}_w \in \mathbb{R}^{n_w \times n_{g_w}}$, $\mathbf{c}_w \in \mathbb{R}^{n_w}$, $\mathbf{A}_w \in \mathbb{R}^{n_{c_w} \times n_{g_w}}$, $\mathbf{b}_w \in \mathbb{R}^{n_{c_w}}$, $\mathbf{G}_v \in \mathbb{R}^{n_v \times n_{g_v}}$, $\mathbf{c}_v \in \mathbb{R}^{n_v}$, $\mathbf{A}_v \in \mathbb{R}^{n_{c_v} \times n_{g_v}}$, $\mathbf{b}_v \in \mathbb{R}^{n_{c_v}}$, $\mathbf{u}_k \in \mathbb{R}^{n_u}$, and $\mathbf{y}_k \in \mathbb{R}^{n_y}$. For simplicity, we define $m = n + n_w$, $m_g = n_g + n_{g_w}$, $m_c = n_c + n_{c_w}$, $\delta_n = n - n_y$, $\delta_w = n_{g_w} - n_{c_w}$, $\delta_v = n_{g_v} - n_{c_v}$, and $\tilde{\delta} = m_g^2 - m_c^2$. Moreover, we consider that scalar real function and scalar inclusion function evaluations have complexity $O(1)$. These correspond to evaluations of the nonlinear dynamics in (1) and its derivatives using real and interval arithmetic, respectively. The complexities of the basic operations on zonotopes and constrained zonotopes used to derive the figures in Table 1 can be found in Appendix.

The dominant terms in the prediction step of CZMV come from the computation of the interval hulls of X and W and the CZ-inclusions $\triangleleft(\mathbf{J}, X - \mathbf{h})$ and $\triangleleft(\mathbf{J}_w, W - \mathbf{h}_w)$ in Theorem 2 and Remark 4. In the case of CZFO, the dominant terms come from the computation of the interval matrices $\tilde{\mathbf{Q}}^{[q]}$, the interval hull of $Z = X \times W$, and the CZ-inclusion $\triangleleft(\mathbf{L}, (\mathbf{c} - \mathbf{h}) \oplus 2\mathbf{G}B_\infty(\mathbf{A}, \mathbf{b}))$ in Theorem 3. Note that the worst-case complexities of the prediction steps of our methods are higher than the zonotope methods, while the update steps are cheaper due to the generalized intersection (22). Even so, the complexities of the proposed methods are polynomial. For a simplified analysis, assuming that all of the variables in Table 1 increase linearly with n, the total complexities for ZMV, ZFO, CZMV and CZFO are $O(n^4)$, $O(n^5)$, $O(n^5)$, and $O(n^8)$, respectively. On the other hand, even basic polytope operations are known to be exponential (Hagemann, 2015). Besides, despite the higher complexities of CZMV and CZFO in comparison to the zonotope methods, they provide more accurate enclosures as shown in the next section.

5. Numerical examples

This section presents numerical results for the two new set-valued state estimation methods enabled by the results in the previous section. The imposed limits on the complexity of the sets used are described separately for each example below.

5.1. Example 1

To demonstrate the effect of the different choices of $\mathbf{h}$, we first analyze one iteration of the prediction step for the nonlinear

[6] Note that this choice may lead to the same value of $\mathbf{h}$ provided by *C1*, but X is described by a different CG-rep with center $\mathbf{h}$. If this point is not in X, $\bar{\mathbf{h}}$ can be chosen as the point obtained from Proposition 1 instead.

[7] We use the standard $O(\cdot)$ notation defined in Cormen, Leiserson, Rivest, and Stein (2009).

Table 1
Computational complexity $O(\cdot)$ of the state estimators.

Step	ZMV	ZFO
Prediction	$n^2 n_g + n n_w n_{g_w}$	$n(m^2 m_g + m m_g^2)$
Update	$n_y(n^3(m_g+n)+n^2(m_g+n)^2+n_u+n_v n_{g_v})$	$n_y(n^3(m_g^2+n)+n^2(m_g^2+n)^2+n_u+n_v n_{g_v})$
Reduction	$n^2(m_g+n)+n(n_{g_w}+n)(m_g+n)$	$n^2(m_g^2+n)+n(m_g^2+n)^2$
Step	**CZMV**	**CZFO**
Prediction	$n^2 n_g + n n_w n_{g_w} + (n n_g + n_c)(n_g+n_c)^3 + (n_w n_{g_w} + n_{c_w})(n_{g_w}+n_{c_w})^3$	$n(m^2 m_g + m m_g^2) + (m m_g + m_c)(m_g+m_c)^3$
Update	$n_y n(m_g+n) + n_y n_u + n_y n_v n_{g_v}$	$n_y n(m_g^2+n) + n_y n_u + n_y n_v n_{g_v}$
Reduction	$(n_{c_w}+n_{c_v}+n_y)(m_g+m_c+n_{g_v}+n_{c_v}+n+n_y)^3$ $+(n+n_c)^2(n_g+\delta_n+\delta_w+\delta_v)+(n+n_c)(\delta_n+\delta_w+\delta_v)(n_g+\delta_n+\delta_w+\delta_v)$	$(m_c^2+n_{c_v}+n_y)(m_g^2+m_c^2+n_{g_v}+n_{c_v}+n+n_y)^3$ $+(n+n_c)^2(\bar{\delta}+\delta_n+\delta_v)+(n+n_c)(\bar{\delta}+\delta_n+\delta_v)^2$

system (Raimondo, Riverso, Summers, Jones, Lygeros, & Morari, 2012)

$$x_{1,k} = 3x_{1,k-1} - \frac{x_{1,k-1}^2}{7} - \frac{4x_{1,k-1}x_{2,k-1}}{4+x_{1,k-1}} + w_{1,k-1},$$
$$x_{2,k} = -2x_{2,k-1} + \frac{3x_{1,k-1}x_{2,k-1}}{4+x_{1,k-1}} + w_{2,k-1}, \tag{23}$$

with

$$X_0 = \left\{ \begin{bmatrix} 0.2 & 0.4 & 0.2 \\ 0.2 & 0 & -0.2 \end{bmatrix}, \begin{bmatrix} -1 \\ 1 \end{bmatrix}, \begin{bmatrix} 2 & 2 & 2 \end{bmatrix}, -3 \right\}, \tag{24}$$

where $\mathbf{w}_k \in \mathbb{R}^2$ denotes process uncertainties, which are zero in this first scenario.

Fig. 1 shows the constrained zonotope X_0 and the enclosures of the one-step reachable set obtained by Theorem 2 using *C1*–*C4*. Since the complexity of the enclosure for *C4* is higher than for the other methods (see Proposition 2), the reduction methods in Scott et al. (2016) were used to reduce the number of generators and constraints in this enclosure to match the other methods before comparison. In this example, the choice of $\mathbf{h}$ has a moderate impact in the enclosure computed by Theorem 2, with *C2* providing the least conservative result, as expected. Therefore, *C2* is employed in Theorem 2 henceforth.

Fig. 1 also shows the enclosures of the one-step reachable set obtained by Theorem 3 with *C1*–*C4*. Clearly, the enclosures produced by Theorem 3 are strongly affected by the choice of $\mathbf{h}$, with *C4* providing the least conservative result. In addition, note that the enclosures provided by the first-order Taylor extension are more conservative than those obtained by the mean value extension. However, experience with zonotopes and intervals (see Raimondo et al. (2012) for detailed examples) suggests that the relative merits of these two methods will depend on the dynamics of the system, as well as the shape and size of the set X_0, and the maximum allowed number of generators and constraints. This is corroborated by the next results.

We consider now the linear measurement equation

$$\begin{bmatrix} y_{1,k} \\ y_{2,k} \end{bmatrix} = \begin{bmatrix} 1 & 0 \\ -1 & 1 \end{bmatrix} \begin{bmatrix} x_{1,k} \\ x_{2,k} \end{bmatrix} + \begin{bmatrix} v_{1,k} \\ v_{2,k} \end{bmatrix}, \tag{25}$$

with bounds $\|\mathbf{w}_k\|_\infty \leq 0.4$ and $\|\mathbf{v}_k\|_\infty \leq 0.4$, where $\mathbf{v}_k \in \mathbb{R}^2$ denote measurement uncertainties. The initial states $\mathbf{x}_0$ are bounded by the zonotope[8]

$$X_0 = \left\{ \begin{bmatrix} 0.1 & 0.2 & -0.1 \\ 0.1 & 0.1 & 0 \end{bmatrix}, \begin{bmatrix} 0.5 \\ 0.5 \end{bmatrix} \right\}. \tag{26}$$

To generate process measurements, (23) was simulated with $\mathbf{x}_0 = (0.8, 0.65) \in X_0$ and process and measurement uncertainties drawn from uniform random distributions. The number of generators and constraints of the constrained zonotopes was limited to 20 and 5, respectively, while the number of generators of the zonotopes was limited to 20. Fig. 2 shows the results of the initial update step using the intersection algorithm in Bravo et al. (2006) and the generalized intersection (22) computed using (10), which yields a constrained zonotope. Clearly, since the generalized intersection is not a symmetric set, it cannot be described by a zonotope. In contrast, the resulting constrained zonotope corresponds to the exact intersection, providing far less conservative bounds in the first update step.

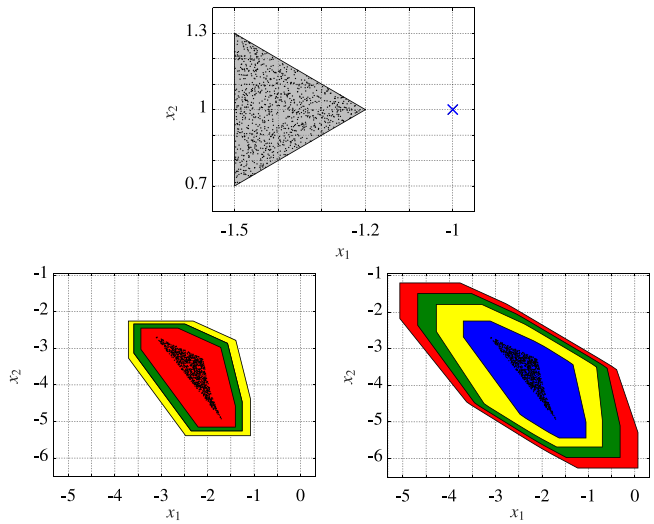

Fig. 1. Top: The constrained zonotope X_0 with '×' denoting its center. Left: Enclosures obtained by applying Theorem 2 to (23). Right: Enclosures obtained by applying Theorem 3 to (23). The real vector $\mathbf{h}$ is determined by *C1* (green), *C2* (red), *C3* (yellow), and *C4* (blue). For the mean value extension (left), *C4* is overlapped with *C1*. Black dots denote uniform samples from X_0 propagated through (23). (For interpretation of the references to color in this figure legend, the reader is referred to the web version of this article.)

Fig. 3 shows the first four time steps of CZMV with $\mathbf{h}$ given by *C2* in a scenario without process uncertainties ($\mathbf{w}_k = \mathbf{0}$). For comparison, the zonotopes computed using ZMV are also depicted. CZMV provides much less conservative enclosures than ZMV for this example, demonstrating the effectiveness of the proposed nonlinear state estimation strategy.

Fig. 4 shows the radii (half the length of the longest edge of the interval hull) of the sets provided by CZMV using *C2* and ZMV over 100 time steps considering process disturbances. Since (23) is affine in $\mathbf{w}_k$, the enclosure $Z \supseteq \boldsymbol{\mu}(\mathbf{h}, W)$ in Theorem 2 was computed as described at the end of Remark 4. CZMV provided less conservative bounds than the zonotopes computed by ZMV, with a CZMV-to-ZMV average radius ratio (ARR, i.e., the ratio of the radius of the CZMV set at k over the ZMV set at k averaged over all time steps k) of only 51.4%. Fig. 4 also compares the

[8] Note that X_0, W and V are expressed as zonotopes for the purpose of a fair comparison with the zonotope methods.

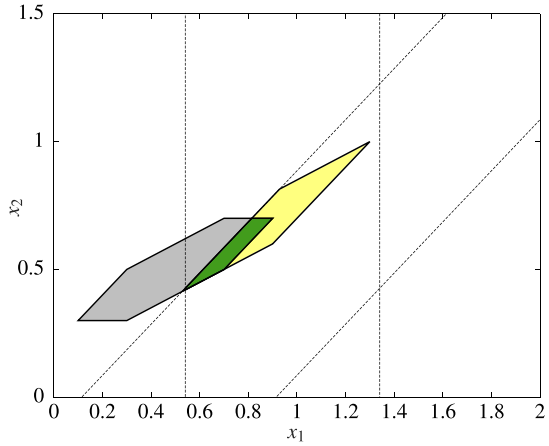

Fig. 2. The initial set X_0 (gray), the initial bounded uncertain measurements (dashed lines), the intersection computed as in Bravo et al. (2006) (yellow), and the constrained zonotope (green) computed by (22). (For interpretation of the references to color in this figure legend, the reader is referred to the web version of this article.)

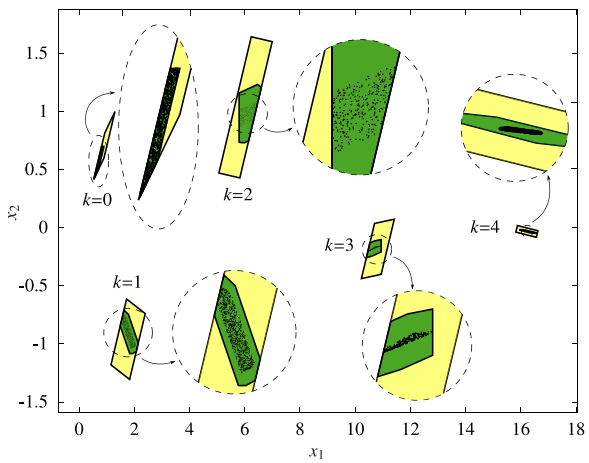

Fig. 3. Results from the first four time steps of set-valued state estimation (after update) using the constrained zonotopic method CZMV (green) and the zonotopic method ZMV (yellow). Black dots denote uniform samples from X_0 propagated through (23) that are consistent with the current measurement. (For interpretation of the references to color in this figure legend, the reader is referred to the web version of this article.)

radii of the update sets computed by ZFO and CZFO with $\mathbf{h}$ given by *C4*. As in the previous case, CZFO provides less conservative bounds than ZFO, with the CZFO-to-ZFO ARR being only 53.66%. The size of the sets provided by CZMV and CZFO were quite similar, with CZFO being less conservative (the CZFO-to-CZMV ARR was 98.75%). In both experiments, the number of generators and constraints were limited to 20 and 5, respectively. The ARR for different numbers of constraints are shown in Table 2, with the average computed considering in addition simulations with different numbers of generators. Execution times are shown in Table 3. These were obtained using MATLAB 9.1 with CPLEX 12.8 and INTLAB 9, in a laptop with 8 GB RAM and an Intel Core i7 4510U 3.1 GHz processor.

The use of constrained zonotopes in CZMV and CZFO results in sets that are slightly more complex than those generated by ZMV and ZFO (specifically, the set description involves five equality constraints that are not present in the zonotopes from ZMV and ZFO). However, this example shows that this increase in complexity is compensated by greatly improved accuracy.

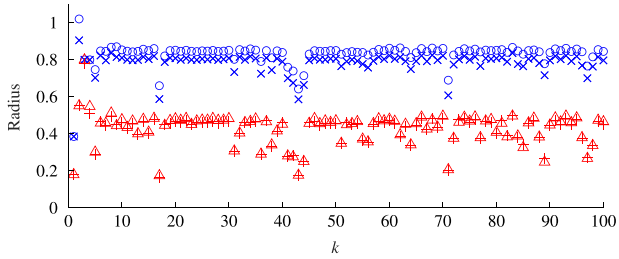

Fig. 4. Radii of the update sets obtained by applying CZMV (△), ZMV (○), CZFO (+), and ZFO (×) to (23) with process disturbances.

Table 2
Average radius ratio of the estimators with varying numbers of constraints. Each average is taken over 3 separate simulations using $n_g \in \{8, 12, 20\}$.

n_c	CZMV/ZMV	CZFO/ZFO	CZFO/CZMV
1	54.1%	59.8%	104.5%
3	51.6%	54.0%	99.0%
5	51.6%	53.7%	98.5%

Table 3
Average total times per iteration of the estimators with varying numbers of constraints. Each average is taken over 30 separate simulations using $n_g \in \{8, 12, 20\}$. Times spent only on complexity reduction are shown in parenthesis.

n_c	ZMV	ZFO	CZMV	CZFO
0	5.79 (0.24) ms	14.03 (2.93) ms	–	–
1	–	–	19.2 (1.6) ms	76.4 (57.1) ms
3	–	–	20.7 (1.8) ms	4.28 (4.26) s
5	–	–	22.5 (1.9) ms	8.93 (8.91) s

5.2. Example 2

Consider the quadrotor unmanned aerial vehicle (UAV) described in Mistler, Benallegue, and M'Sirdi (2001) with state vector $\boldsymbol{\zeta} = [x\ y\ z\ u\ v\ w\ \phi\ \theta\ \psi\ p\ q\ r]^T$, where $[x\ y\ z]^T$ is the position of the UAV with respect to the inertial frame, $[u\ v\ w]^T$ is the velocity vector expressed in the inertial frame, $[\phi\ \theta\ \psi]^T$ are Euler angles describing the orientation of the UAV, and $[p\ q\ r]^T$ is the angular velocity vector expressed in the body frame. The equations of motion are (Mistler et al., 2001):

$$\dot{\boldsymbol{\zeta}} = \begin{cases} \dot{x} = u, \\ \dot{y} = v, \\ \dot{z} = w, \\ \dot{u} = \frac{1}{m}(\cos\psi\sin\theta\cos\phi + \sin\psi\sin\phi)U_1 + \frac{1}{m}D_x, \\ \dot{v} = \frac{1}{m}(\sin\psi\sin\theta\cos\phi - \cos\psi\sin\phi)U_1 + \frac{1}{m}D_y, \\ \dot{w} = -g + \frac{1}{m}(\cos\theta\cos\phi)U_1 + \frac{1}{m}D_z, \\ \dot{\phi} = p + q\sin\phi\tan\theta + r\cos\phi\tan\theta, \\ \dot{\theta} = q\cos\phi - r\sin\phi, \\ \dot{\psi} = q\sin\phi\sec\theta + r\cos\phi\sec\theta, \\ \dot{p} = \frac{I_{yy} - I_{zz}}{I_{xx}}qr + \frac{l}{I_{xx}}U_2, \\ \dot{q} = \frac{I_{zz} - I_{xx}}{I_{yy}}pr + \frac{l}{I_{yy}}U_3, \\ \dot{r} = \frac{I_{xx} - I_{yy}}{I_{zz}}pq + \frac{1}{I_{zz}}U_4, \end{cases} \tag{27}$$

where m, I_{xx}, I_{yy}, I_{zz}, and l are physical parameters, g is the gravitational acceleration, U_1 is the total thrust generated by

Table 4
Measured variables with error bounds.

Sensor	Variables	Noise bounds
GPS	$\{x, y\}$	$\pm$ 0.15 m
Barometer	$\{z\}$	$\pm$ 0.51 m
IMU	$\{\phi, \theta, \psi\}$	$\pm$ $2.618{\cdot}10^{-3}$ rad
	$\{p, q, r\}$	$\pm$ $16.558{\cdot}10^{-3}$ rad/s

the propellers, U_2 is the difference of thrusts between the left and right propellers, U_3 is the difference of thrusts between the front and back propellers, U_4 is the difference of torques between clockwise and counter-clockwise turning propellers, and $\mathbf{d} = [D_x \;\; D_y \;\; D_z]^T$ are disturbance forces applied to the UAV with $\|\mathbf{d}\|_\infty \leq 1$. The experiment consists in obtaining guaranteed bounds on the system states $\boldsymbol{\zeta}$ while the quadrotor UAV tracks a vertical helix trajectory defined by the reference values $x^{\text{ref}}(t) = \frac{1}{2}\cos\left(\frac{t}{2}\right)$, $y^{\text{ref}}(t) = \frac{1}{2}\sin\left(\frac{t}{2}\right)$, $z^{\text{ref}}(t) = 1 + \frac{t}{10}$, $\psi^{\text{ref}} = \frac{\pi}{3}$, subject to the disturbance forces described by $D_x = 1$ N for $t \in [5, 15)$ s, $D_y = 1$ N for $t \in [8, 15)$ s, and $D_z = 1$ N for $t \in [10, 15)$ s. These forces are zero otherwise.

The dynamic feedback controller in Mistler et al. (2001) is used to track the reference trajectory above.[9] The simulation parameters are $m = 0.7$ kg, $l = 0.3$ m, $I_{xx} = I_{yy} = I_{zz} = 1.2416$ kg·m^2, $g = 9.81$ m/s^2. We consider a realistic scenario in which the available measurements are provided by sensors located at the quadrotor UAV, which include: (i) a Global Positioning System (GPS); (ii) a barometer; and (iii) an Inertial Measurement Unit (IMU). The measurements are affected by bounded uncertainties as described in Table 4. The velocity vector $[u \;\; v \;\; w]^T$ is not measured.

The nonlinear equations (27) were discretized by Euler approximation with sampling time 0.01 s. The initial states $\boldsymbol{\zeta}_0$ are bounded by $X_0 = \{\mathbf{G}_0, \mathbf{0}\}$, where $\mathbf{G}_0 = \text{diag}\left(2, 2, 2, 1, 1, 1, \frac{\pi}{6}, \frac{\pi}{6}, \frac{\pi}{2}, \frac{\pi}{12}, \frac{\pi}{12}, \frac{\pi}{12}\right)$. To generate process measurements, the discrete-time dynamics were simulated with $\boldsymbol{\zeta}_0 = [0.5 \;\; 0 \;\; 1 \;\; \mathbf{0}_{1\times5} \;\; \pi/3 \;\; \mathbf{0}_{1\times3}]^T \in X_0$ and process and measurement noises drawn from uniform distributions. Fig. 5 shows the trajectory performed by the quadrotor UAV along with the interval hulls[10] of the enclosures computed by the methods CZMV and ZMV, projected onto (x, y, z)-axes. CZMV was implemented with $\mathbf{h}$ given by *C2*, and since (27) is also affine in $\mathbf{w}_k \triangleq \mathbf{d}_k$, Theorem 3 was implemented with $Z \supseteq \boldsymbol{\mu}(\mathbf{h}, W)$ computed as described at the end of Remark 4. The number of constraints and generators of the computed constrained zonotopes was limited to 40 and 12, respectively, while the number of generators of the computed zonotopes was limited to 40.

The interval hulls of the constrained zonotopes obtained by CZMV were smaller than those from ZMV, demonstrating the accuracy of the proposed method. Fig. 6 shows the radii of the constrained zonotopes and zonotopes computed by CZMV and ZMV, respectively. Both algorithms were capable of providing tight bounds on the system states $\boldsymbol{\zeta}_k \in \mathbb{R}^{12}$. Nevertheless, CZMV provided less conservative bounds than ZMV, even for a high-order nonlinear dynamical system such as (27) (the CZMV-to-ZMV ARR was 74.41%). Finally, Fig. 7 compares the radii of the update sets

[9] In this experiment, the control action is computed using the real states $\boldsymbol{\zeta}_k$. The approach in Rego et al. (2018a) can be used for feedback connection using a point that belongs to $\hat{X}_k$.

[10] The conversion from CG-rep to H-rep (see Scott et al. (2016)) for the purposes of exact drawing is intractable for the constrained zonotopes in this example.

Table 5
Average radius ratio of the estimators with varying numbers of constraints. Each average is taken over 3 separate simulations with $n_g \in \{25, 30, 40\}$.

n_c	CZMV/ZMV	CZFO/ZFO	CZFO/CZMV
3	82.5%	82.2%	99.9%
6	76.7%	77.1%	100.7%
12	75.0%	74.8%	99.7%

Table 6
Average total times per iteration of the estimators with varying numbers of constraints. Each average is taken over 15 separate simulations using $n_g \in \{25, 30, 40\}$. Times spent only on complexity reduction are shown in parenthesis.

n_c	ZMV	ZFO	CZMV	CZFO
0	53.3 (1.0) ms	174.2 (54.2) ms	–	–
3	–	–	104.7 (7.3) ms	266.9 (128.6) ms
6	–	–	109.5 (8.4) ms	615.0 (471.6) ms
12	–	–	127.8 (12.3) ms	2.62 (2.46) s

computed by ZFO and CZFO with $\mathbf{h}$ given by *C3*.[11] Once again, CZFO provided less conservative bounds than ZFO (the CZFO-to-ZFO ARR was 74.45%). The results from CZMV and CZFO were again very similar, with CZMV providing marginally better results (the CZMV-to-CZFO ARR was 99.93%). The ARR for different numbers of constraints are shown in Table 5, with the average computed considering in addition simulations with different numbers of generators. Execution times are shown in Table 6. Note that most of the CZFO execution times are smaller than the ones presented in Table 3. This might be counter-intuitive since the current example has more state variables. However the use of *C4* in Example 1 results in a relatively more complex enclosure and therefore requires a much higher execution time for generator reduction and constraint elimination. Note that in this example, the computational times of the state estimators were greater than the considered sampling time of 0.01 s. Nevertheless, this fact does not invalidate the obtained results since these were run in a numerical simulation. Better times can be achieved by optimized implementation of the algorithms and using more powerful hardware, for instance. Besides, note that even though the current execution times of CZMV and CZFO would in principle prevent their use in fast applications, the improved accuracy can significantly reduce the number of time steps required for guaranteed fault detection and isolation for systems in which execution time is not critical.

6. Conclusions and future work

This paper proposed two novel approaches for set-valued state estimation of nonlinear discrete-time systems with unknown-but-bounded process and measurement uncertainties. A mean value extension and a first-order Taylor extension were developed based on constrained zonotopes, a generalization of zonotopes capable of describing strongly asymmetric convex sets. In addition, measurement data were effectively taken into account by means of generalized intersection, which resulted in far less conservative results than existing methods based on zonotopes. The accuracy of the proposed methods was demonstrated by means of three numerical examples, the third one being an experiment with a quadrotor UAV, considering a realistic scenario with uncertain measurements provided by sensors located on the aircraft. In the latter, execution times were longer than the considered sampling time. Nevertheless, an optimized implementation of the methods, as well as more powerful hardware,

[11] The increased complexity of the constrained zonotopes provided by *C4* proved to be intractable for this example.

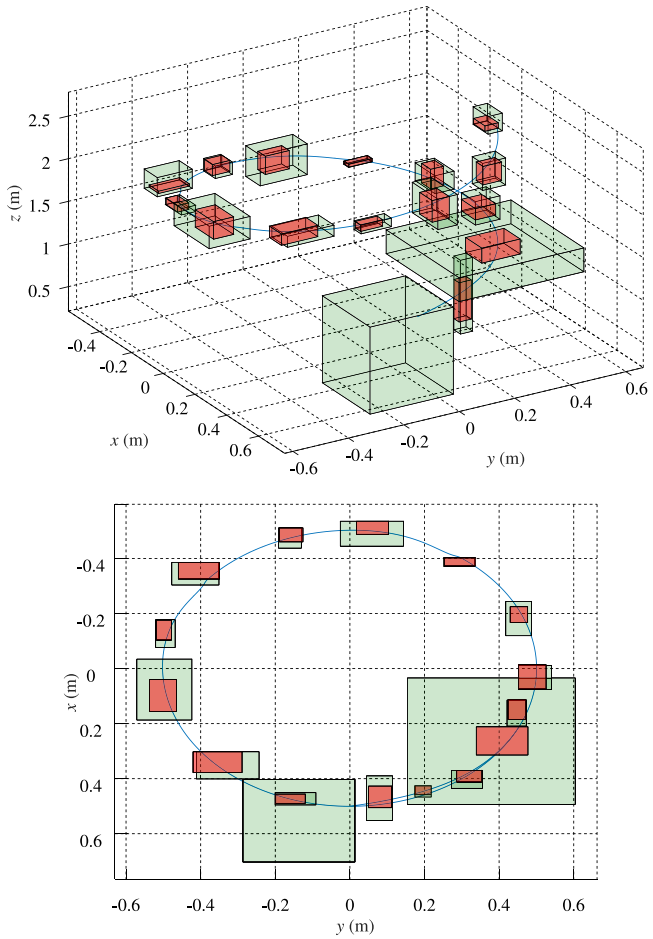

Fig. 5. The trajectory performed by the quadrotor UAV (solid line) and the interval hulls of the constrained zonotopes (red boxes) and zonotopes (green boxes) estimated by CZMV and ZMV, respectively, projected onto (x, y, z). (For interpretation of the references to color in this figure legend, the reader is referred to the web version of this article.)

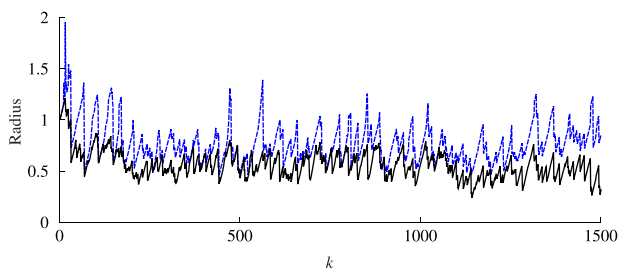

Fig. 6. Radii of the update sets computed by CZMV (—) and ZMV (– –) for the quadrotor UAV experiment.

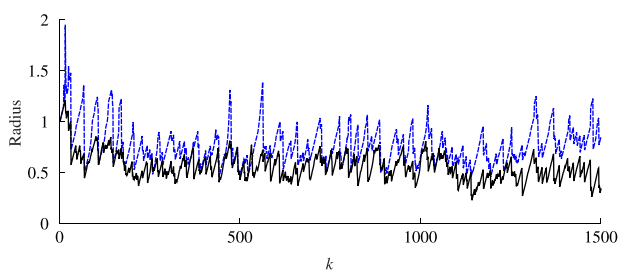

Fig. 7. Radii of the update sets computed by CZFO (—) and ZFO (– –) for the quadrotor UAV experiment.

Table 7
Computational complexity $O(\cdot)$ of basic operations.

Operation	Zonotopes	Constrained zonotopes
Linear mapping	$nn_g n_r$	$nn_g n_r$
Minkowski sum	n	n
Generalized intersection	–	$nn_g n_r + n_r n_{g_r}$
Interval hull	nn_g	$nn_g(n_g + n_c)^3$
Set inclusion	nn_g	$nn_s n_g + n_c(n_g + n_c)^3 + nn_g^2 n_c$
Closest point	–	$(n + n_g)(n + n_g + n_c)^3$
Change center	–	$n_g(n + n_g)^3 + n_g^2 n_c$
Generator reduction	$n^2 n_g + k_g n n_g$	$(n + n_c)^2 n_g + k_g(n + n_c)n_g$
Constraint elimination	–	$k_c(n_g + n_c)^3 + k_c n n_g^2$

implementation in C++ and parallelization techniques, could be used to achieve better times. This issue is left as a future work seeking the practical implementation in a real aircraft.

Appendix. Computational complexity details

Table 7 shows the computational complexity of the basic operations used in the zonotope and constrained zonotope methods. These complexities assume generic inputs with dimensions $\mathbf{R} \in \mathbb{R}^{n_r \times n}$ in (4); $Y = \{\mathbf{G}_y, \mathbf{c}_y, \mathbf{A}_y, \mathbf{b}_y\}$ in (6), with $\mathbf{G}_y \in \mathbb{R}^{n_r \times n_{g_r}}$, $\mathbf{c}_y \in \mathbb{R}^{n_r}$, $\mathbf{A}_y \in \mathbb{R}^{n_{c_r} \times n_{g_r}}$, and $\mathbf{b}_y \in \mathbb{R}^{n_{c_r}}$; $\mathbf{J} \in \mathbb{IR}^{n_s \times n}$ in Theorem 1; $X = \{\mathbf{G}_x, \mathbf{c}_x\}$ or $X = \{\mathbf{G}_x, \mathbf{c}_x, \mathbf{A}_x, \mathbf{b}_x\}$, with $\mathbf{G}_x \in \mathbb{R}^{n \times n_g}$, $\mathbf{c}_x \in \mathbb{R}^n$, $\mathbf{A}_x \in \mathbb{R}^{n_c \times n_g}$, and $\mathbf{b}_x \in \mathbb{R}^{n_c}$; k_g and k_c are the number of generators and constraints removed in the order reduction process, respectively. 'Set inclusion' refers to the zonotope inclusion in Alamo et al. (2005) for zonotopes and the CZ-inclusion (Theorem 1) for constrained zonotopes. 'Closest point' and 'Change center' correspond to Propositions 1 and 2, respectively, which are LPs. For the latter, the bounds $\tilde{\boldsymbol{\xi}}^{\mathrm{L}}, \tilde{\boldsymbol{\xi}}^{\mathrm{U}}$ are obtained using Algorithm 1 in Scott et al. (2016). Note that the interval hull of zonotopes does not require the solution of LPs (see Remark 3 in Kühn (1998)). In addition, we consider that each LP is solved at least with the performance of the simplex method presented in Kelner and Spielman (2006), which is $O(N_d N_c^3)$ with N_d and N_c the number of decision variables and constraints, respectively. Note that these numbers can be inferred for each respective LP directly from Table 7. For a detailed derivation of the computational complexities in Tables 1 and 7, please see the supplementary material in Rego, Raffo, Scott, and Raimondo (2019).

References

Alamo, T., Bravo, J., & Camacho, E. (2005). Guaranteed state estimation by zonotopes. *Automatica*, *41*(6), 1035–1043.

Alamo, T., Bravo, J. M., Redondo, M. J., & Camacho, E. F. (2008). A set-membership state estimation algorithm based on DC programming. *Automatica*, *44*(1), 216–224.

Althoff, M. (2013). Reachability analysis of nonlinear systems using conservative polynomialization and non-convex sets. *Hybrid Systems: Computation and Control*, 173–182.

Althoff, M., & Krogh, B. H. (2011). Zonotope bundles for the efficient computation of reachable sets. In *Proc. of the 50th IEEE conference on decision and control*, (pp. 6814-6821).

Boyd, S., & Vandenberghe, L. (2004). *Convex optimization*. Cambridge.

Bravo, J. M., Alamo, T., & Camacho, E. F. (2006). Bounded error identification of systems with time-varying parameters. *IEEE Transactions on Automatic Control*, *51*(7), 1144–1150.

Chabane, S. B., Maniu, C. S., Alamo, T., Camacho, E., & Dumur, D. (2014). Improved set-membership estimation approach based on zonotopes and ellipsoids. In *Proc. of the 2014 European control conference* (pp. 993-998).

Chisci, L., Garulli, A., & Zappa, G. (1996). Recursive state bounding by parallelotopes. *Automatica*, *32*(7), 1049–1055.

Combastel, C. (2003). A state bounding observer based on zonotopes, In *Proc. of the 2003 European control conference* (pp. 2589-2594).

Combastel, C. (2005). A state bounding observer for uncertain non-linear continuous-time systems based on zonotopes. In *Proc. of the 44th IEEE conference on decision and control, and 2005 european control conference* (pp. 7228-7234).

Combastel, C. (2015). Merging Kalman filtering and zonotopic state bounding for robust fault detection under noisy environment. In *Proc. of the 9th IFAC symposium on fault detection, supervision and safety for technical processes* (pp. 289-295).

Combastel, C., Zhang, Q., & Lalami, A. (2008). Fault diagnosis based on the enclosure of parameters estimated with an adaptive observer. In *Proc. of the 17th IFAC world congress* (pp. 7314-7319).

Cormen, T. H., Leiserson, C. E., Rivest, R. L., & Stein, C. (2009). *Introduction to algorithms* (3rd ed.). Cambridge.

Durieu, C., Walter, E., & Polyak, B. (2001). Multi-input multi-output ellipsoidal state bounding. *Journal of Optimization Theory and Applications*, *111*(2), 273–303.

Girard, A., & Guernic, C. L. (2008). Efficient reachability analysis for linear systems using support functions. In *Proc. of the 17th IFAC world congress* (pp. 8966-8971).

Goodarzi, F. A., & Lee, T. (2017). Global formulation of an extended Kalman filter on SE(3) for geometric control of a quadrotor UAV. *Journal of Intelligent and Robotic Systems*, *88*(2), 395–413.

Hagemann, W. (2015). Efficient geometric operations on convex polyhedra, with an application to reachability analysis of hybrid systems. *Mathematics in Computer Science*, *9*(3), 283–325.

Jaulin, L. (2009a). A nonlinear set membership approach for the localization and map building of underwater robotics. *IEEE Transactions on Robotics*, *25*(1), 88–98.

Jaulin, L. (2009b). Robust set-membership state estimation; application to underwater robotics. *Automatica*, *45*(1), 202–206.

Jaulin, L. (2016). Inner and outer set-membership state estimation. *Reliable Computing*, *22*, 47–55.

Kelner, J. A., & Spielman, D. A. (2006). A randomized polynomial-time simplex algorithm for linear programming. In *Proc. of the 38th annual ACM symposium on theory of computing* (pp. 51–60).

Kieffer, M., Jaulin, L., & Walter, E. (1998). Guaranteed nonlinear state estimation using interval analysis. In *Proc. of the 37th conference on decision and control* (pp. 3966-3971).

Kopetzki, A.-K., Schürmann, B., & Althoff, M. (2017). Methods for order reduction of zonotopes. In *Proc. of the 56th conference on decision and control* (pp. 5626-5633).

Kühn, W. (1998). Rigorously computed orbits of dynamical systems without the wrapping effect. *Computing*, *61*(1), 47–67.

Le, V. T. H., Stoica, C., Alamo, T., Camacho, E. F., & Dumur, D. (2013). Zonotopic guaranteed state estimation for uncertain systems. *Automatica*, *49*(11), 3418–3424.

Mistler, V., Benallegue, A., & M'Sirdi, N. K. (2001). Exact linearization and noninteracting control of a 4 rotors helicopter via dynamic feedback. In *Proc. of the 10th IEEE international workshop on robot and human interactive communication* (pp. 586-593).

Moore, R. E., Kearfott, R. B., & Cloud, M. J. (2009). *Introduction to interval analysis*. Philadelphia, PA, USA: SIAM.

Platzer, A., & Clarke, E. M. (2007). The image computation problem in hybrid systems model checking. In *Proc. of the international workshop on hybrid systems: computation and control* (pp. 473-486).

Polyak, B. T., Nazin, S. A., Durieu, C., & Walter, E. (2004). Ellipsoidal parameter or state estimation under model uncertainty. *Automatica*, *40*(7), 1171–1179.

Raimondo, D. M., Marseglia, G. R., Braatz, R. D., & Scott, J. K. (2016). Closed-loop input design for guaranteed fault diagnosis using set-valued observers. *Automatica*, *74*, 107–117.

Raimondo, D. M., Riverso, S., Summers, S., Jones, C. N., Lygeros, J., & Morari, M. (2012). A set-theoretic method for verifying feasibility of a fast explicit nonlinear model predictive controller. In R. Johansson, & A. Rantzer (Eds.), *Distributed decision making and control* (pp. 289–311). London: Springer London.

Rego, B. S., & Raffo, G. V. (2019). Suspended load path tracking control using a tilt-rotor UAV based on zonotopic state estimation. *Journal of the Franklin Institute*, *356*(4), 1695–1729.

Rego, B. S., Raffo, G. V., Scott, J. K., & Raimondo, D. M. (2019). Supplementary material. In *Guaranteed methods based on constrained zonotopes for setvalued state estimation of nonlinear discrete-time systems*, https://arxiv.org/abs/1908.09950.

Rego, B. S., Raimondo, D. M., & Raffo, G. V. (2018). Path tracking control with state estimation based on constrained zonotopes for aerial load transportation. In *Proc. of the 57th IEEE conference on decision and control* (pp. 1979-1984).

Rego, B. S., Raimondo, D. M., & Raffo, G. V. (2018). Set-based state estimation of nonlinear systems using constrained zonotopes and interval arithmetic. In *Proc. of the 2018 European control conference* (pp. 1584-1589).

Saeedi, S., Trentini, M., Seto, M., & Li, H. (2016). Multiple-robot simultaneous localization and mapping: A review. *Journal of Field Robotics*, *33*(1), 3–46.

Santos, M. A., Rego, B. S., Raffo, G. V., & Ferramosca, A. (2017). Suspended load path tracking control strategy using a tilt-rotor UAV. *Journal of Advanced Transportation*, *2017*, 1–22.

Schweppe, F. (1968). Recursive state estimation: Unknown but bounded errors and system inputs. *IEEE Transactions on Automatic Control*, *13*(1), 22–28.

Scott, J. K., Raimondo, D. M., Marseglia, G. R., & Braatz, R. D. (2016). Constrained zonotopes: a new tool for set-based estimation and fault detection. *Automatica*, *69*, 126–136.

Shamma, J. S., & Tu, K.-Y. (1997). Approximate set-valued observers for nonlinear systems. *IEEE Transactions on Automatic Control*, *42*(5), 648–658.

Shamma, J. S., & Tu, K.-Y. (1999). Set-valued observers and optimal disturbance rejection. *IEEE Transactions on Automatic Control*, *44*(2), 253–264.

Vicino, A., & Zappa, G. (1996). Sequential approximation of feasible parameter sets for identification with set membership uncertainty. *IEEE Transactions on Automatic Control*, *41*(6), 774–785.

Walter, E., & Piet-Lahanier, H. (1989). Exact recursive polyhedral description of the feasible parameter set for bounded-error models. *IEEE Transactions on Automatic Control*, *34*(8), 911–915.

Wan, J., Sharma, S., & Sutton, R. (2018). Guaranteed state estimation for nonlinear discrete-time systems via indirectly implemented polytopic set computation. *IEEE Transactions on Automatic Control*, *63*(12), 4317–4322.

Yang, X., & Scott, J. K. (2018). Accurate set-based state estimation for nonlinear discrete-time systems using differential inequalities with model redundancy. In *Proc. of the 57th IEEE conference on decision and control* (pp. 680-685).

Yang, X., & Scott, J. K. (2018). A comparison of zonotope order reduction techniques. *Automatica*, *95*, 378–384.

Zhao, S., Huang, B., & Liu, F. (2015). Fault detection and diagnosis of multiple-model systems with mismodeled transition probabilities. *IEEE Transactions on Industrial Electronics*, *62*(8), 5063–5071.

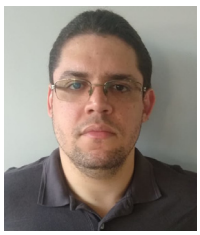

Brenner S. Rego is currently a Ph.D. candidate in Electrical Engineering at the Federal University of Minas Gerais, Brazil. He received his B.S. in Electrical Engineering from the Federal University of Goiás, in 2014, and his M.S. in Electrical Engineering from the Federal University of Minas Gerais, in 2016. He is the author or co-author of diverse papers published in refereed journals and conference proceedings. His current research interests include active fault diagnosis and fault-tolerant control, set-valued state estimation, modeling and control of unmanned aerial vehicles, and aerial load transportation.

Guilherme V. Raffo was born in Porto Alegre, Brazil. He received the B.Sc. degree in automation and control engineering from the Pontifical Catholic University of Rio Grande do Sul, Brazil, in 2002, his specialist degree in industrial automation from the Federal University of Rio Grande do Sul, Brazil, in 2003, his M.Sc. degree in electrical engineering from the Federal University of Santa Catarina, Brazil, in 2005, his M.Sc. degree in automation, robotics and telematic in 2007 and his Ph.D. degree in 2011, both from the University of Seville, Spain, and was a Postdoctoral fellow in 2011–2012 at the Federal University of Santa Catarina, Brazil. He is currently an Associate Professor at Federal University of Minas Gerais, Brazil. He is the author or coauthor of more than 90 publications including journal papers, book chapters, and conference proceedings. His current research interests include robust control, nonlinear control, $\mathcal{H}_\infty$ control theory, predictive control, set-membership state estimation, fault-tolerant control, unmanned aerial vehicles, robotics, and underactuated systems.

Joseph K. Scott is an Associate Professor in the Department of Chemical and Biomolecular Engineering at the Georgia Institute of Technology. He received his B.S. (2006) in Chemical Engineering from Wayne State University, and his M.S. (2008) and Ph.D. (2012) in Chemical Engineering from MIT. His honors include the 2012 Best Paper Award from the Journal of Global Optimization, the 2016 W. David Smith, Jr. Award from the Computing and Systems Technology Division of the AIChE, the 2014–2016 Automatica Paper Prize from the International Federation of Automatic Control, and the 2016 Air Force Young Investigator Research Program Award. His research interests include dynamical systems, optimization theory, simulation and optimization of chemical processes, advanced process control, and fault diagnosis.

Davide M. Raimondo (M'19) received the Ph.D. in Electronics, Computer Science and Electrical Engineering from the University of Pavia, Italy, in 2009. From January 2009 to December 2010 he was a postdoctoral fellow in the Automatic Control Laboratory, ETH Zurich, Switzerland. From December 2010 to May 2015 he was assistant professor at University of Pavia. He has held visiting positions at the Massachusetts Institute of Technology, University of Seville, Vienna University of Technology, University of Konstanz. Prof. Raimondo is currently an associate professor and head of the educational Process Control Laboratory in the Department of Electrical, Computer and Biomedical Engineering at University of Pavia, Italy. He is the author or co-author of more than 85 papers published in refereed journals, edited books, and refereed conference proceedings. He serves/served as subject editor for the journals IEEE Transactions on Control Systems Technology (2019-) and Optimal Control Applications and Methods (2015–2018) and as CEB member of IEEE Control Systems Society. His current research interests include advanced battery management systems, active fault diagnosis and fault-tolerant control, model predictive control and optimization. In 2017, Prof. Raimondo, with co-authors, received the 2014–2016 Automatica Paper Prize Award.